Supporting Online Material for

Higher-Order Cellular Information Processing with Synthetic RNA Devices

Maung Nyan Win and Christina D. Smolke*

*To whom correspondence should be addressed. E-mail: smolke@cheme.caltech.edu

Published 17 October 2008, *Science* **322**, 456 (2008)
DOI: 10.1126/science.1160311

This PDF file includes:

Materials and Methods

Plasmid construction, cloning, and cell strains

Using standard molecular biology techniques (*S1*), the plasmid pRzS, harboring the yeast-enhanced green fluorescence protein (yEGFP) (*S2*) under the control of a GAL1-10 promoter, was constructed as previously described (*S3*) and employed as a universal vector for the characterization of all higher-order RNA devices. All RNA device constructs were generated by PCR amplification using the appropriate oligonucleotide templates and primers. All oligonucleotides were synthesized by Integrated DNA Technologies (IDT). Single ribozyme devices (SI 2 and 3) were cloned into two unique restriction sites, *Avr*II and *Xho*I, 3 nucleotides downstream of the stop codon of yEGFP and upstream of an ADH1 terminator sequence. For dual ribozyme devices (SI 1), the second single-input gate including spacer sequences was cloned immediately downstream of the first single-input gate in the second restriction site (*Xho*I). The functions and sequences of all devices are listed in SOM text S6. Representative secondary structures and sequences are illustrated in figs. S16 and S17. Cloned plasmids were transformed into an electrocompetent *Escherichia coli* strain, DH10B (Invitrogen) and all constructs were confirmed by subsequent sequencing (Laragen, Inc). Confirmed plasmid constructs were transformed into a *Saccharomyces cerevisiae* strain (W303 *MATα his3-11,15 trp1-1 leu2-3 ura3-1 ade2-1*) using standard lithium acetate procedures (*S4*).

RNA secondary structure prediction, free energy calculation, and corresponding proposed mechanism

RNAstructure 4.2 (http://rna.urmc.rochester.edu/rnastructure.html) was used to predict the secondary structures of all RNA devices and their corresponding thermodynamic properties as previously described (*S3*). Prediction of the secondary structures of the RNA devices based on SI 1 and 2 has been previously described (*S3*). RNA sequences that are predicted to adopt at least two stable conformations (ribozyme-active and -inactive) were constructed and characterized for their functional activity. Our design strategy is based on engineering competitive hybridization events within the transmitter components that enable the devices to distribute between two primary

conformations: one in which the ligand-binding pocket is not formed (input cannot bind the sensor), and the other in which the ligand-binding pocket is formed (input can bind the sensor). Input binding shifts the distribution to favor the input-bound conformation as a function of increasing input concentration and is translated to a change in activity of the ribozyme, where a ribozyme-active state results in self-cleavage of the ribozyme. A representative schematic of an Inverter gate is illustrated in fig. S2. For RNA devices composed of two internal gates linked through a single ribozyme stem (SI 3), RNA sequences that are predicted to adopt generally at least three stable conformations of interest (Fig. 4, A and C) were constructed and characterized for their functional activity. The device design strategies and their regulatory mechanisms closely follow those described above.

In vivo assays for characterization of RNA device properties and fluorescence quantification

S. cerevisiae cells harboring plasmids carrying appropriate RNA devices were grown in synthetic complete medium supplemented with an appropriate amino acid dropout solution and sugar (2% raffinose, 1% sucrose) overnight at 30^{o}C (*S3*). The overnight cell cultures were back-diluted into fresh medium to an OD_{600} of approximately 0.1. At the time of back-dilution, an appropriate volume of galactose (2% final concentration) or an equivalent volume of water were added to the cultures for the induced and non-induced controls, respectively. In addition, an appropriate volume of concentrated input stock dissolved in medium, or an equivalent volume of the medium (no input control) was added to the cultures (to the appropriate final concentration of theophylline, tetracycline, or both inputs, as described in the figure legends). The back-diluted cells were then grown to an OD_{600} of 0.8-1.0 or for a period of approximately 6 hours before measuring output GFP levels on a Cell Lab Quanta SC flow cytometer (Beckman Coulter). Output GFP expression level distributions within the cell populations were measured using the following settings: 488 nm laser line, 525 nm bandpass filter, and a PMT setting of 5.83. Fluorescence data were collected from 10,000 viable cell counts of each culture sample under low flow rates. A non-induced cell population was used to set a background level, and cells exhibiting fluorescence above this background

level are defined as the GFP-expressing cell population. The gene expression activity of a device construct is reported as the mean fluorescence value of the gated GFP-expressing cell population.

Characterization of device higher-order information processing properties

Device responses are reported as the arithmetic difference between the gene expression activities of a construct in the absence and presence of the appropriate molecular inputs in fluorescence units of expression, unless otherwise indicated. 1 unit expression was defined as the gene expression activity of the construct carrying the parental active ribozyme sTRSV relative to that of the inactive ribozyme sTRSV Contl in the absence of input (*S3* and see below for the mathematical description). The expression activity of the sTRSV construct is ~2% of that of the construct carrying the inactive ribozyme control sTRSV Contl or the full transcriptional range of 50 units of expression. The following equations provide the device output data evaluation and presentation schemes used in this work.

1 unit expression (U_{ex}) = the gene expression activity of the parental active ribozyme sTRSV relative to that of the inactive ribozyme sTRSV Contl in the absence of input

$= r_0/c_0$

$\approx r_L/c_L$

where r and c represent the expression activities of the active sTRSV and inactive sTRSV Contl ribozyme constructs, respectively, and the subscripts, 0 and L, indicate the absence and presence of the appropriate molecular input(s), respectively.

Device signal (S_d) = the gene expression activity of an RNA device relative to that of sTRSV Contl

$= s/c$

where s represents the expression activity of the device. To report device signal as a percentage, the device signal (S_d) was multiplied with 100%. To report device signal in units of expression, the device signal (S_d) was divided by U_{ex}. Device response ($R_{d,L}$) is

the arithmetic difference between the device signals in the absence and presence of the appropriate molecular input(s) (denoted as $S_{d,0}$ and $S_{d,L}$, respectively) and mathematically represented as $R_{d,L} = S_{d,L} - S_{d,0}$, unless otherwise indicated. In all of the above equations, r, c, and s values were taken from at least three independent experiments.

Cooperative binding activities of RNA devices were determined using the Hill equation: $y = y_{\max} x^{n_H} / \left(x^{n_H} + K^{n_H} \right)$ where y is the gene expression activity at an input concentration x, y_{max} is the maximum gene expression activity or saturation level, and n_H and K represent the Hill coefficient and the ligand concentration at the half maximal response, respectively. Experiments demonstrate that the device responses begin to saturate at 10 mM theophylline, such that Hill coefficients were determined by normalizing the device response to the response at 10 mM theophylline and plotting log [fraction expressed (or repressed) / (1 - fraction expressed (or repressed))] versus log [input concentration], where the slope represents the Hill coefficient (n_H). All fluorescence data and mean ±s.d. are reported from at least three independent experiments.

Supporting Text

Text S1: RNA device response properties and standards in data presentation

There has been significant effort directed to the characterization of natural and engineered RNA devices. These efforts have resulted in important descriptions and demonstrations of RNA devices; however, the work is often reported through different metrics and standards. Standard means of reporting the characterized device properties are needed to accurately evaluate, compare, and appreciate the functional properties of the diverse RNA devices that have been developed or will be developed.

The RNA device properties that characterize the performance of a device include output swing (R_d, absolute difference of the dynamic range; here reported as device response), output fold induction or repression ($S_{d,L}/S_{d,0}$, ratio of the dynamic range), baseline expression ($S_{d,0}$, expression activity in the absence of input ligand; here reported as output basal signal), and input swing (input concentration over which device output

changes) (see Materials and Methods and Text S1 fig. 1 for details). Text S1 fig. 1 provides a pictorial description of how device response data were evaluated in this work. In order to fully characterize the dynamic range of an RNA device, either the baseline expression and the output swing or the baseline expression and the output fold induction (repression) should be reported. However, such dynamic range data cannot be compared across different genetic constructs and systems which can alter the observed response of an RNA device. For example, different organisms will have different transcriptional capacities; different regulated genes will have different fold expression/activity levels (e.g., enzyme-based reporters exhibit turnover of a substrate and an amplified fold induction range relative to fluorescent protein-based reporters); and different promoters will have different fold transcriptional ranges. Therefore, reporting device response properties relative to standards are critical to enabling comparison of the performance of different devices within the context of different genetic constructs and systems.

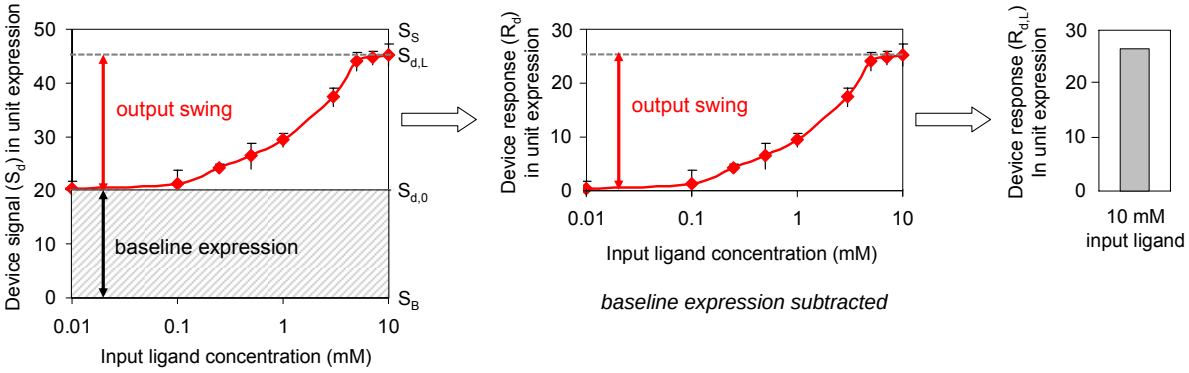

Text S1 fig. 1. A pictorial description of evaluation of device response data in this work.

Here, we propose the use of two standards in RNA device characterization: (i) the gene expression activity from the genetic construct (including promoter, gene, etc.) in the absence of the RNA device (100%; signal standard, S_S (Text S1 fig. 1)), and (ii) the gene expression activity in the absence of the genetic construct (0%; background standard, S_B (Text S1 fig. 1)). The proposed standards allow researchers to determine the performance of the RNA device across the full transcriptional range of a specified promoter, without any non-specific effects that an inactive RNA device might exhibit due to its location relative to other components in the genetic construct and its secondary structure. The use

of reference standards is important because the RNA device (and therefore its performance) is coupled to other components in the genetic construct, including a promoter. Therefore, components can be changed to alter the baseline expression level relative to the signal standard as appropriate for a given application.

A device architecture that enables modification of baseline expression activities of single-input gates is shown in Fig. 2A, where multiple single-input gates are coupled in a device to alter both the baseline expression and output swing. We selected single-input gates with varying baseline expression activities to demonstrate the effects of gate coupling on baseline expression from the device (Fig. 2B; SOM text S2). We have previously reported on a tuning strategy targeted to the transmitter component that can be used to build single-input gates with lower baseline expression activities (Buffer8; ~12%) (*3*). Therefore, the combination of these two strategies (transmitter tuning and gate coupling) results in devices that exhibit much lower baseline expression activities (2xBuffer8; ~7%). We report output swing (device response) and baseline expression (device signal in the absence of input) in Fig. 2B to demonstrate the tuning of baseline expression. To simplify data presentation and focus on the response of the RNA devices to inputs, we report only output swing for most of the other devices in the main figures, and report baseline expression activities in the Supporting Online Material (table S1). In addition, another straightforward way to alter the baseline expression from an RNA device is to alter the promoter that it is coupled to. For example, in the systems reported here all devices are coupled to a very strong promoter (GAL1-10). If we replaced that promoter with a weaker promoter, the baseline expression activity would be much lower relative to the signal standard.

With the goal of integrating RNA devices into different genetic circuits (composed of various biological components), such standardized characterization information is critical to match properties of the components in the circuit to achieve the desired system response. RNA devices do not necessarily need to exhibit output swings that span the full transcriptional range of a very strong promoter in order to be biologically relevant. Many endogenous proteins and enzymes are expressed at levels much lower than that obtained from the stronger promoters commonly used in recombinant work. In addition, proteins can exhibit very different thresholds of titratable

function depending on their activities, such that a very low baseline expression is not always necessary. Even natural riboswitches may not be used to titrate enzyme concentrations across their full response curves, as that would require cells to regulate input metabolite concentrations to these regulators over a ~10^4-10^5-fold range. As such, an important property of RNA devices is their ability to be tuned to exhibit different device response properties using (1) energetic tuning strategies targeted to the transmitter component (*S3*); (2) coupled single-input gates (Fig. 2B); and (3) component matching (*S5, S6*). These strategies provide important flexibility in tuning RNA device response to fit applications with different performance requirements. We have demonstrated previously that the output swings and baseline expression activities exhibited by RNA devices are biologically relevant, specifically in the application of intracellular detection of metabolic concentrations (where an output swing outside the noise in gene expression is important) and the regulation of cell growth/death (where the ability to titrate the output swing across a threshold concentration of the regulated protein is important) (*S3*). In addition, there are many other examples where noncoding RNAs play key regulatory roles in controlling biological function without exhibiting regulatory ranges across the full transcriptional range of the promoter system of the genetic construct (*S7-S10*).

Text S2: Predicted and observed response properties of coupled single-input gates

Coupled single-input gate devices (SI 1) are composed of single-input gates that are expected to act independently. Independent function of the single-input gates results in several predictions, regarding the response properties of such coupled gate devices relative to the single-input gates, previously described by Welz and Breaker in a tandem riboswitch system composed of two independent riboswitches (*S11*). However, the predicted changes in the device response properties were not shown to be exhibited by the naturally-occurring functional counterpart (*S11*), and are examined here for the synthetic devices.

The first predicted property of a coupled single-input gate device is that it will exhibit decreased basal output signals from the single-input gate. The expected decrease in basal output signal can be predicted from the single-input gate responses and follows a

straightforward probability determination that both gates are in the ribozyme-inactive state (requiring AND behavior):

$$p_d = p_1 * p_2$$

where p is the fraction in the ribozyme-inactive state (determined as the gene expression activity relative to that of the ribozyme-inactive control, here reported as device signal); subscripts 1, 2, and d indicate single-input gate 1, single-input gate 2, and the coupled single-input gate device, respectively. The predicted and measured basal output signals are shown in table S1. For most of the coupled single-input gate devices the predicted and measured basal output signals match well, supporting the independent function of the single-input gates. There are two coupled single-input gate devices, both composed of L2cm4, for which there is not a strong match between the predicted and measured values. The results indicate that L2cm4 may not function independently when coupled in a higher-order device. L2cm4 has a transmitter component that functions through a different mechanism than the other single-input gates examined here (*S3*), specifically through a helix-slipping mechanism (*S12*). This information transmission mechanism requires the presence of non-Watson-Crick base pairs within the transmitter component, which may result in weaker device structural stability, potentially allowing non-specific interactions with surrounding sequences and thus interfering with the independent function of this single-input gate.

The effect of decreased basal output signal, has also been predicted to result in an increased device response for such systems (*S11*). This would generally be true under situations in which the input concentration is saturating to the response of the system and irreversible rates do not dominate reversible rates. In the experimental systems examined here, the input ligands may not be at fully saturating concentrations due to transport limitations across the cell membrane and toxicity of the input molecules at high concentrations. In addition, in certain systems the irreversible rate of ribozyme cleavage may compete with the reversible rate of conformational switching.

The second and third predicted properties of coupled single-input gate devices apply to devices that respond to the same inputs (SI 1.1) and apply to the characteristics of the input-response curve. The second property is associated with the sensitivity of the device to input concentration. As previously pointed out, devices that couple Inverter

gates (repress gene expression) are predicted to trigger a gene control response at lower input concentrations (*S11, S13*). This behavior results from such coupled Inverter gate devices functioning essentially through OR behavior, as the independent activation of either single-input gate through input binding results in the repression of gene expression from a transcript. However, devices that couple Buffer gates (activate gene expression) are expected to trigger a gene control response at higher input concentrations, as the independent activation of both gates through input binding (AND behavior) is required to activate gene expression from a transcript.

The third property is associated with the slope of the response curve over ranges in gene expression. Coupled single-input gate devices are predicted to result in a more 'digital' response curve (*S11*), where the same output dynamic range can be achieved with a lower change in input concentration. This effect should be true for both coupled Inverter and Buffer gate devices, although the actual increase in the 'digital' nature of the response curve is predicted to be quite low (*S11*). In addition, this effect would only generally be true under situations in which the input concentration is saturating to the response of the system. For example, at lower input concentrations (i.e., input concentrations lower than the midway point of the input swing), the coupled Inverter gate device is predicted to have a higher slope than the single-input gate, whereas the coupled Buffer gate device is predicted to have a lower slope than the single-input gate. Therefore, the predicted effects on the slope of the response curve are anticipated to be small.

We measured the ligand response curves of two representative coupled single-input gate devices and their single-gate counterparts (text S2 fig. 1). The coupled Inverter gate device (2xInverter1) exhibited a response at slightly lower concentrations of input than the single Inverter gate (Inverter1), whereas the coupled Buffer gate device (2xBuffer1) exhibited a response at slightly higher concentrations of input than the single Buffer gate (Buffer1). However, the observed changes in the response curves were very slight, such that strong conclusions on the effects of gate coupling on the input-response curves cannot be made.

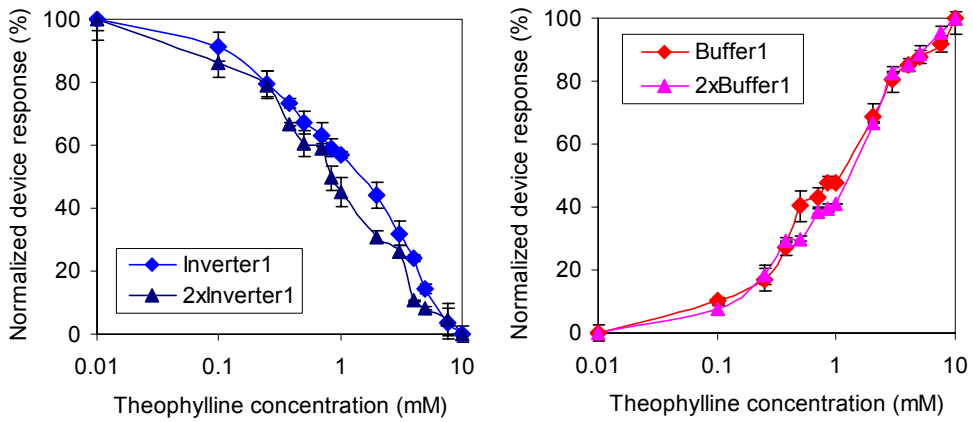

Text S2 fig. 1. The normalized device response over varying input concentrations of representative coupled gate devices (2xInverter1, left; 2xBuffer1, right) constructed through SI 1.1 and their corresponding single-gate device counterparts (Inverter1, Buffer1). The device response is normalized to the device response in 10 mM theophylline.

Text S3: Layered architectures extend the information processing capabilities of SI 1

The first assembly scheme based on signal integration within the 3' UTR provides modular composition frameworks for two basic logic operators, AND and NOR gates. Additional logic operators may be desired, including NAND and OR gates. One way in which to directly obtain these logic operations from the assembled operations in SI 1 is to invert the output from the AND and NOR gates, respectively (text S3 fig. 1). For example, the resulting output of the AND and NOR gates can be an Inverter device such as a repressor protein (*S14*) or an inhibitory noncoding RNA (*S15*) that acts on a separately encoded gene product resulting in the desired NAND and OR operations, respectively. However, this proposed framework results in a layered architecture, which may have less desirable properties such as loss of signal and longer signal processing times. Alternative assembly strategies for obtaining additional logic operations that result in non-layered architectures are described in the manuscript.

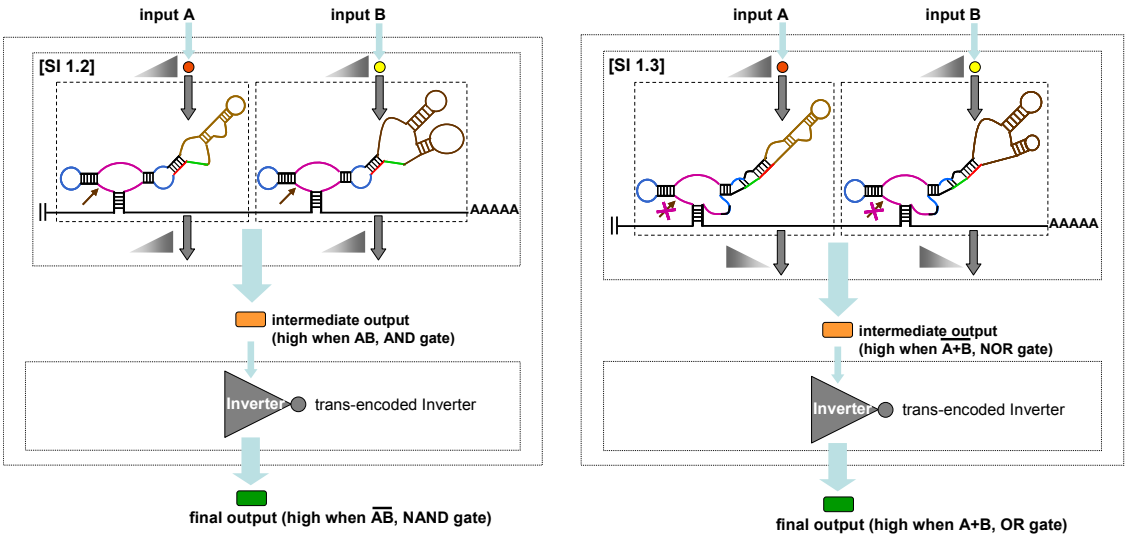

Text S3 fig. 1. Schematic representation of layered architectures that extend the information processing capabilities of SI 1. Left, schematic illustrating a NAND operation by inverting the output of an AND gate. Right, schematic illustrating an OR operation by inverting the output of a NOR gate.

Text S4: Non-layered architectures (SI 2, SI 3) for an OR operation

The second assembly scheme based on signal integration at the ribozyme core (SI 2) should be as flexible a composition framework as that specified for integration within the 3' UTR (SI 1). For example, SI 2 can be implemented to construct a higher-order RNA device capable of performing an OR operation by coupling internal Buffer gates responsive to different molecular inputs to stems I and II of the ribozyme (SI 2.2, text S4 fig. 1). This device is expected to exhibit low output only in the absence of both inputs, as both internal Buffer gates favor the ribozyme-active state. While such a logic operation is theoretically possible, its construction is currently limited by the lack of one necessary component of this device - an internal Buffer gate coupled to stem I. Efforts are currently underway to generate such components. Therefore, SI 2 can provide logic operations that are not attainable through SI 1 with non-layered architectures.

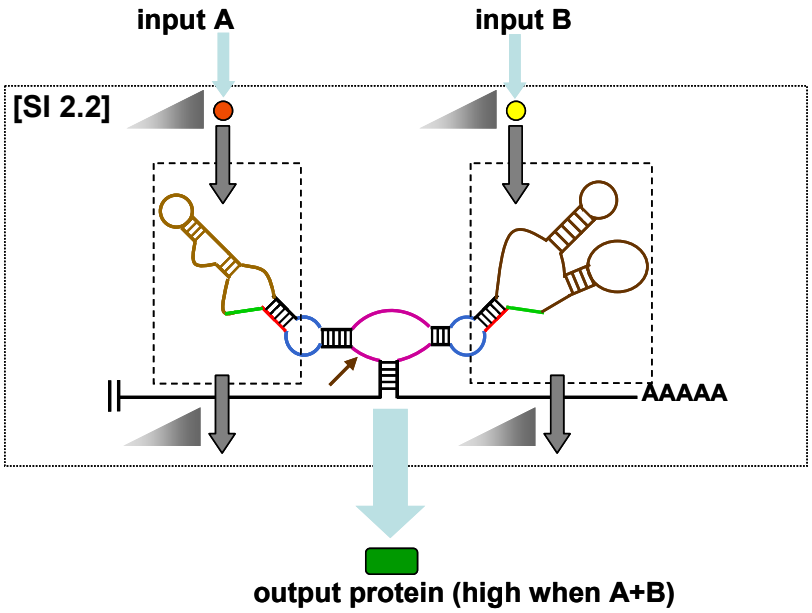

Text S4 fig. 1. Schematic representation of an RNA device based on SI 2 that functions as an OR gate.

Alternatively, devices that perform an OR operation were constructed through SI 3 (signal integration through a single ribozyme stem) by coupling a theophylline-responsive internal Buffer gate (IG1) and a tetracycline-responsive internal Inverter gate (IG2) at stem II (text S4 fig. 2A). The assembly scheme is similar to that used to construct devices that perform an AND operation, described in Fig. 4A, except that the energetic requirements for switching between the conformational states were different. This RNA device (SI 3.3) assumed the conformation in which the binding pockets for both inputs are formed (text S4 fig. 2A) with a lower energetic requirement than an AND gate device ($\Delta\Delta G_{IG12}$ in SI 3.3 < $\Delta\Delta G_{IG2}$+ $\Delta\Delta G_{IG1}$ in SI 3.1), effectively allowing either input to bind to its corresponding sensor. In this composition, IG1 changed the state of the RNA device to favor the ribozyme-inactive state in the presence of either input or both, resulting in high device output (text S4 fig. 2B). We constructed two OR gate devices, tc/theo-On1 and tc/theo-On2, based on different IG2 transmitter components.

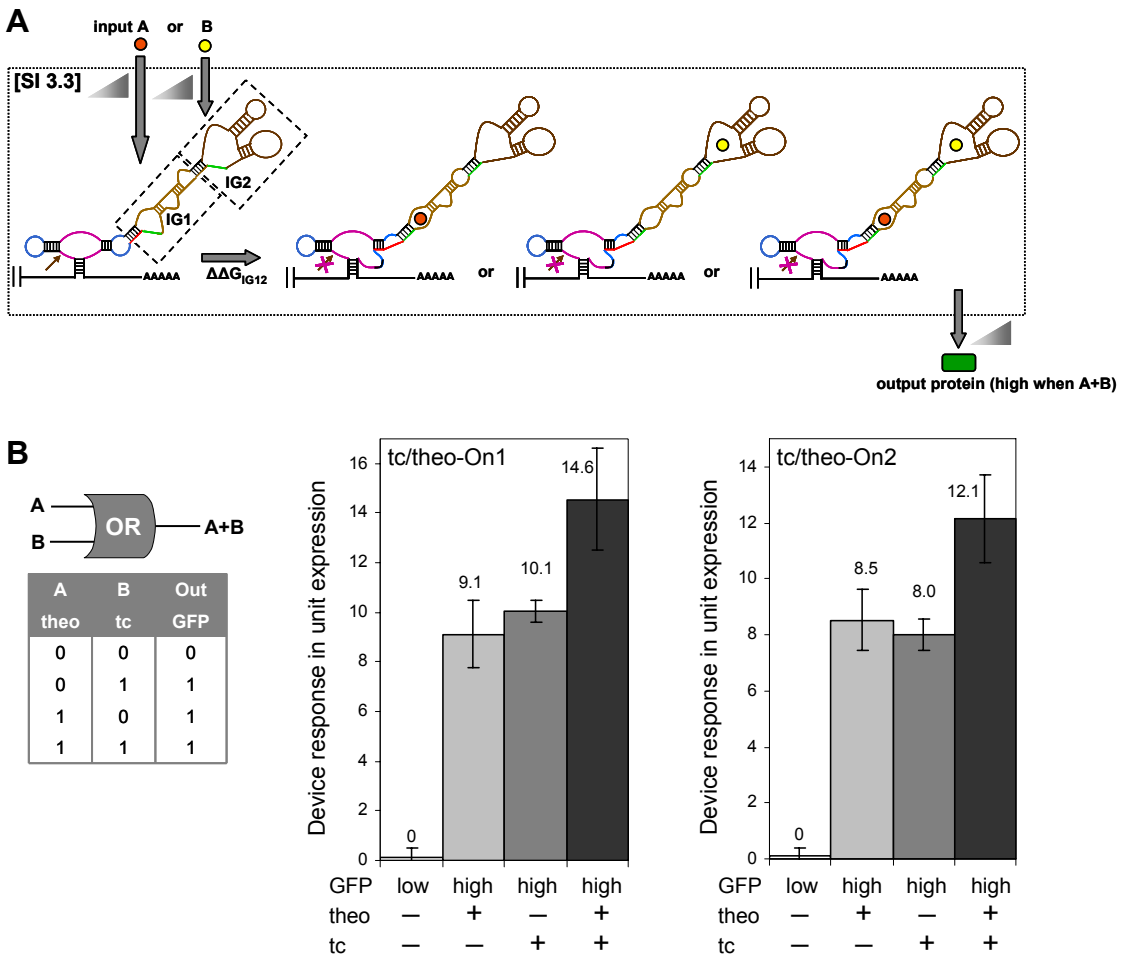

Text S4 fig. 2. OR gate devices based on SI 3. **(A)** Schematic representation of an RNA device that performs an OR operation by coupling internal Buffer (IG1) and Inverter (IG2) gates responsive to different input molecules to a single ribozyme stem. **(B)** The device response and truth table of OR gates (tc/theo-On1 and tc/theo-On2) based on SI 3.3. Device response under different input conditions (theo or tc (-), 0 mM; theo (+), 10 mM; tc (+), 0.25 mM) is reported as the difference between expression activity in the absence of both inputs and that at the indicated input conditions.

Text S5: Programming cooperativity through multiple sensor-transmitter components

Cooperativity in biological molecules is often a result of multiple binding sites that transit from a low-affinity state to a high-affinity state as more ligands occupy the available binding sites. In RNA devices composed of two internal gates to the same input, although the sensor components exhibit similar input binding affinities (K_{apt}), their

effective affinities are a combined effect of the sensor affinity (K_{apt}) and the energetic requirements for the device to switch between two states (K_{IG}), the latter of which can be programmed into the transmitter component ($\Delta\Delta G_{IG}$). Thus, the difference in free energies between states 1 and 3 ($\Delta\Delta G_{IG2}$+ $\Delta\Delta G_{IG1}$) represents an energetic contribution which lowers the effective binding affinity of IG1 to its input. The difference in free energies between states 1 and 2 ($\Delta\Delta G_{IG2}$) represents a lower energetic contribution to the effective binding affinity of IG2 to its input, such that the effective binding affinity of IG2 is higher than that of IG1. However, binding of input to IG2 lowers the energetic contribution to IG1 to the difference in free energies between states 2 and 3 ($\Delta\Delta G_{IG1}$), resulting in an increase in the effective binding affinity of the device as a result of input binding to IG2. The RNA device design is expected to result in a larger change in the device response as input concentrations increase and IG1 transits from a lower affinity state to a higher affinity state. By programming the energetic differences between the different conformational states ($\Delta\Delta G_{IG2}$ and $\Delta\Delta G_{IG1}$), we can program the degree of cooperativity exhibited by the device (table S2).

Text S6: *Device sequences*

The functions and sequences of all devices used in this work are described below. Color schemes in the sequences correspond to those in the schematic device diagrams: purple, catalytic core of the ribozyme or actuator component; blue, loop regions of the actuator component; brown, aptamer or sensor component; green and red, strands within the transmitter component that participate in the competitive hybridization event, respectively; orange, strands within the transmitter component that participate in a helix slipping event; italicized, spacer sequences; underlined, restriction sites.

Single-input gates

Single-input Buffer gates

L2bulge1 (Buffer1 from Fig. 2B)
5’CCTAGG*AAACAAACAAA*GCTGTCACCGGATGTGCTTTCCGGTCTGATGAGTCC
GTGTCCATACCAGCATCGTCTTGATGCCCTTGGCAGGGACGGGACGAGGACG
AAACAGC*AAAAAGAAAAATAAAAA*CTCGAG

L2bulge5 (Buffer5 from Fig. 2B)
5’CCTAGG*AAACAAACAAA*GCTGTCACCGGATGTGCTTTCCGGTCTGATGAGTCC
GTGTCCAATACCAGCATCGTCTTGATGCCCTTGGCAGTGGACGGGACGAGGA
CGAAACAGC*AAAAAGAAAAATAAAAA*CTCGAG

L2bulge8 (Buffer8 from Fig. 2B)
5’CCTAGG*AAACAAACAAA*GCTGTCACCGGATGTGCTTTCCGGTCTGATGAGTCC
GTTGTCCATACCAGCATCGTCTTGATGCCCTTGGCAGGGACGGGACGGAGGA
CGAAACAGC*AAAAAGAAAAATAAAAA*CTCGAG

L2bulge9
5’CCTAGG*AAACAAACAAA*GCTGTCACCGGATGTGCTTTCCGGTCTGATGAGTCC
GTTGTCCAATACCAGCATCGTCTTGATGCCCTTGGCAGTGGATGGGGACGGA
GGACGAAACAGC*AAAAAGAAAAATAAAAA*CTCGAG

L2bulge1tc (Buffer-tc from Fig. 2B)
5’CCTAGG*AAACAAACAAA*GCTGTCACCGGATGTGCTTTCCGGTCTGATGAGTCC
GTGTCCAAAACATACCAGATTTCGATCTGGAGAGGTGAAGAATTCGACCACC
TGGACGGGACGAGGACGAAACAGC*AAAAAGAAAAATAAAAA*CTCGAG

Single-input Inverter gates

L2bulgeOff1 (Inverter1 from Fig. 2B)
5’CCTAGG*AAACAAACAAA*GCTGTCACCGGATGTGCTTTCCGGTCTGATGAGTCC
GTGTTGCTGATACCAGCATCGTCTTGATGCCCTTGGCAGCAGTGGACGAGGA
CGAAACAGC*AAAAAGAAAAATAAAAA*CTCGAG

L2bulgeOff1tc
5’CCTAGG*AAACAAACAAA*GCTGTCACCGGATGTGCTTTCCGGTCTGATGAGTCC
GTTGTTGAGGAAAACATACCAGATTTCGATCTGGAGAGGTGAAGAATTCGAC
CACCTCCTTATGGGAGGACGAAACAGC*AAAAAGAAAAATAAAAA*CTCGAG

L2bulgeOff2tc
5’CCTAGG*AAACAAACAAA*GCTGTCACCGGATGTGCTTTCCGGTCTGATGAGTCC
GTATGAGGAAAACATACCAGATTTCGATCTGGAGAGGTGAAGAATTCGACCA
CCTCCTTAGAGGAGGACGAAACAGC*AAAAAGAAAAATAAAAA*CTCGAG

L2bulgeOff3tc
5’CCTAGG*AAACAAACAAA*GCTGTCACCGGATGTGCTTTCCGGTCTGATGAGTCC
GTTGATGAGGAAAACATACCAGATTTCGATCTGGAGAGGTGAAGAATTCGAC
CACCTCCTTAGAGGAGGACGAAACAGC*AAAAAGAAAAATAAAAA*CTCGAG

L2cm4 (Inverter4 from Fig. 2B)
5’CCTAGG*AAACAAACAAA*GCTGTCACCGGATGTGCTTTCCGGTCTGATGAGTCC
GTCCTGGATACCAGCATCGTCTTGATGCCCTTGGCAGTCATAGAGGACGAAA
CAGC*AAAAAGAAAAATAAAAA*CTCGAG

L1cm10
5’CCTAGG*AAACAAACAAA*GCTGTCACCGGATGTAAATGATACCAGCATCGTCT
TGATGCCCTTGGCAGCTGCGCTTTCCGGTCTGATGAGTCCGTGAGGACGAAA
CAGC*AAAAAGAAAAATAAAAA*CTCGAG

Higher-order devices (SI 1: signal integration within the 3’ UTR)

Two coupled Buffer or Inverter gates responsive to the same input

2xL2bulge1 (2xBuffer1 from Fig. 2B)
5’CCTAGG*AAACAAACAAA*GCTGTCACCGGATGTGCTTTCCGGTCTGATGAGTCC
GTGTCCATACCAGCATCGTCTTGATGCCCTTGGCAGGGACGGGACGAGGACG
AAACAGCAAAAAGAAAAATAAAAACTCGAG*AAACAAACAAA*GCTGTCACCGG
ATGTGCTTTCCGGTCTGATGAGTCCGTGTCCATACCAGCATCGTCTTGATGCC
CTTGGCAGGGACGGGACGAGGACGAAACAGC*AAAAAGAAAAATAAAAA*CTCGA
G

2xL2bulgeOff1 (2xInverter1 from Fig. 2B)
5’CCTAGG*AAACAAACAAA*GCTGTCACCGGATGTGCTTTCCGGTCTGATGAGTCC
GTGTTGCTGATACCAGCATCGTCTTGATGCCCTTGGCAGCAGTGGACGAGGA
CGAAACAGCAAAAAGAAAAATAAAAACTCGAG*AAACAAACAAA*GCTGTCACC
GGATGTGCTTTCCGGTCTGATGAGTCCGTGTTGCTGATACCAGCATCGTCTTG
ATGCCCTTGGCAGCAGTGGACGAGGACGAAACAGC*AAAAAGAAAAATAAAAA*C
TCGAG

Note: The sequence assembly of other RNA devices based on SI 1.1 (2xBuffer-tc, 2xBuffer8, 2xInverter4, (Buffer1+Buffer5), and (Inverter1+Inverter4)) is identical to that of 2xBuffer1 or 2xInverter1, illustrated above as example templates. Sequences of single-input gates are shown above.

AND gates

AND1 (L2bulge1+L2bulge1tc)
5’CCTAGG*AAACAAACAAA*GCTGTCACCGGATGTGCTTTCCGGTCTGATGAGTCC
GTGTCCATACCAGCATCGTCTTGATGCCCTTGGCAGGGACGGGACGAGGACG
AAACAGCAAAAAGAAAAATAAAAACTCGAG*AAACAAACAAA*GCTGTCACCGG
ATGTGCTTTCCGGTCTGATGAGTCCGTGTCCAAAACATACCAGATTTCGATCT
GGAGAGGTGAAGAATTCGACCACCTGGACGGGACGAGGACGAAACAGC*AAA*
*AAGAAAAATAAAAA*CTCGAG

AND2 (L2bulge9+L2bulge1tc)
5’CCTAGG*AAACAAACAAA*GCTGTCACCGGATGTGCTTTCCGGTCTGATGAGTCC
GTTGTCCAATACCAGCATCGTCTTGATGCCCTTGGCAGTGGATGGGGACGGA
GGACGAAACAGCAAAAAGAAAAATAAAAACTCGAG*AAACAAACAAA*GCTGTC
ACCGGATGTGCTTTCCGGTCTGATGAGTCCGTGTCCAAAACATACCAGATTTC
GATCTGGAGAGGTGAAGAATTCGACCACCTGGACGGGACGAGGACGAAACA
GC*AAAAAGAAAAATAAAAA*CTCGAG

NOR gates

NOR1 (L2bulgeOff1+L2bulgeOff1tc)
5’CCTAGG*AAACAAACAAA*GCTGTCACCGGATGTGCTTTCCGGTCTGATGAGTCC
GTGTTGCTGATACCAGCATCGTCTTGATGCCCTTGGCAGCAGTGGACGAGGA
CGAAACAGCAAAAAGAAAAATAAAAACTCGAG*AAACAAACAAA*GCTGTCACC
GGATGTGCTTTCCGGTCTGATGAGTCCGTTGTTGAGGAAAACATACCAGATTT
CGATCTGGAGAGGTGAAGAATTCGACCACCTCCTTATGGGAGGACGAAACAG
C*AAAAAGAAAAATAAAAA*CTCGAG

NOR2 (L2bulgeOff1+L2bulgeOff2tc)
5’CCTAGG*AAACAAACAAA*GCTGTCACCGGATGTGCTTTCCGGTCTGATGAGTCC
GTGTTGCTGATACCAGCATCGTCTTGATGCCCTTGGCAGCAGTGGACGAGGA
CGAAACAGCAAAAAGAAAAATAAAAACTCGAG*AAACAAACAAA*GCTGTCACC
GGATGTGCTTTCCGGTCTGATGAGTCCGTATGAGGAAAACATACCAGATTTC
GATCTGGAGAGGTGAAGAATTCGACCACCTCCTTAGAGGAGGACGAAACAG
C*AAAAAGAAAAATAAAAA*CTCGAG

Bandpass filter

Bandpass filter1 (L2bulge1+L2bulgeOff1)
5’CCTAGG*AAACAAACAAA*GCTGTCACCGGATGTGCTTTCCGGTCTGATGAGTCC
GTGTCCATACCAGCATCGTCTTGATGCCCTTGGCAGGGACGGGACGAGGACG
AAACAGC*AAAAAGAAAAATAAAAA*CTCGAG*AAACAAACAAA*GCTGTCACCGGATG
TGCTTTCCGGTCTGATGAGTCCGTGTTGCTGATACCAGCATCGTCTTGATGCC
CTTGGCAGCAGTGGACGAGGACGAAACAGC*AAAAAGAAAAATAAAAA*CTCGAG

Higher-order devices (SI 2: signal integration at the ribozyme core through two stems)

NAND gates

NAND1 (L1cm10-L2bulgeOff1tc)
5’CCTAGG*AAACAAACAAA*GCTGTCACCGGATGTAAATGATACCAGCATCGTCT
TGATGCCCTTGGCAGCTGCGCTTTCCGGTCTGATGAGTCCGTTGTTGAGGAAA
ACATACCAGATTTCGATCTGGAGAGGTGAAGAATTCGACCACCTCCTTATGG
GAGGACGAAACAGC*AAAAAGAAAAATAAAAA*CTCGAG

NAND2 (L1cm10-L2bulgeOff3tc)
5’CCTAGG*AAACAAACAAA*GCTGTCACCGGATGTAAATGATACCAGCATCGTCT
TGATGCCCTTGGCAGCTGCGCTTTCCGGTCTGATGAGTCCGTTGATGAGGAAA
ACATACCAGATTTCGATCTGGAGAGGTGAAGAATTCGACCACCTCCTTAGAG
GAGGACGAAACAGC*AAAAAGAAAAATAAAAA*CTCGAG

Higher-order devices (SI 3: signal integration at a single ribozyme stem)

AND gates

AND1 (tc-theo-On1)
5’CCTAGG*AAACAAACAAA*GCTGTCACCGGATGTGCTTTCCGGTCTGATGAGTCC
GTGTCCATACCAGCATCGCTCAAAACATACCAGATTTCGATCTGGAGAGGTG
AAGAATTCGACCACCTGAGTCTTGATGCCCTTGGCAGGGACGGGACGAGGAC
GAAACAGC*AAAAAGAAAAATAAAAA*CTCGAG

AND2 (tc-theo-On2)
5’CCTAGG*AAACAAACAAA*GCTGTCACCGGATGTGCTTTCCGGTCTGATGAGTCC
GTGTCCATACCAGCATCGCTAAAACATACCAGATTTCGATCTGGAGAGGTGA
AGAATTCGACCACCTAGTCTTGATGCCCTTGGCAGGGACGGGACGAGGACGA
AACAGC*AAAAAGAAAAATAAAAA*CTCGAG

AND3 (tc-theo-On3)
5’CCTAGG*AAACAAACAAA*GCTGTCACCGGATGTGCTTTCCGGTCTGATGAGTCC
GTGTCCATACCAGCATCGTGTAAAACATACCAGATTTCGATCTGGAGAGGTG
AAGAATTCGACCACCTACATCTTGATGCCCTTGGCAGGGACGGGACGAGGAC
GAAACAGC*AAAAAGAAAAATAAAAA*CTCGAG

OR gates

OR1 (tc/theo-On1)
5’CCTAGG*AAACAAACAAA*GCTGTCACCGGATGTGCTTTCCGGTCTGATGAGTCC
GTGTCCATACCAGCATCGGGCCTAAAACATACCAGATTTCGATCTGGAGAGG
TGAAGAATTCGACCACCTAGGTTTCTTGATGCCCTTGGCAGGGACGGGACGA
GGACGAAACAGC*AAAAAGAAAAATAAAAA*CTCGAG

OR2 (tc/theo-On2)
5’CCTAGG*AAACAAACAAA*GCTGTCACCGGATGTGCTTTCCGGTCTGATGAGTCC
GTGTCCATACCAGCATCGGTGGTAAAACATACCAGATTTCGATCTGGAGAGG
TGAAGAATTCGACCACCTACCATTCTTGATGCCCTTGGCAGGGACGGGACGA
GGACGAAACAGC*AAAAAGAAAAATAAAAA*CTCGAG

Two coupled internal gates responsive to the same input

theo-theo-On1
5’CCTAGG*AAACAAACAAA*GCTGTCACCGGATGTGCTTTCCGGTCTGATGAGTCC
GTGTCCATACCAGCATCGTTTATACCAGCATCGTCTTGATGCCCTTGGCAGAA
ATCTTGATGCCCTTGGCAGGGACGGGACGAGGACGAAACAGC*AAAAAGAAAAA*
*TAAAAA*CTCGAG

theo-theo-On2
5’CCTAGG*AAACAAACAAA*GCTGTCACCGGATGTGCTTTCCGGTCTGATGAGTCC
GTGTCCATACCAGCATCGTTGAATACCAGCATCGTCTTGATGCCCTTGGCAGT
TGATCTTGATGCCCTTGGCAGGGACGGGACGAGGACGAAACAGC*AAAAAGAA*
*AAATAAAAA*CTCGAG

theo-theo-On3
5’CCTAGG*AAACAAACAAA*GCTGTCACCGGATGTGCTTTCCGGTCTGATGAGTCC
GTGTCCATACCAGCATCGATTGATACCAGCATCGTCTTGATGCCCTTGGCAGC
AGTTCTTGATGCCCTTGGCAGGGACGGGACGAGGACGAAACAGC*AAAAAGAA*
*AAATAAAAA*CTCGAG

theo-theo-On4
5’CCTAGG*AAACAAACAAA*GCTGTCACCGGATGTGCTTTCCGGTCTGATGAGTCC
GTGTCCATACCAGCATCGTATGATACCAGCATCGTCTTGATGCCCTTGGCAGC
GTATCTTGATGCCCTTGGCAGGGACGGGACGAGGACGAAACAGC*AAAAAGAA*
*AAATAAAAA*CTCGAG

theo-theo-On5
5’CCTAGG*AAACAAACAAA*GCTGTCACCGGATGTGCTTTCCGGTCTGATGAGTCC
GTGTCCATACCAGCATCGATCATACCAGCATCGTCTTGATGCCCTTGGCAGGA
TTCTTGATGCCCTTGGCAGGGACGGGACGAGGACGAAACAGC*AAAAAGAAAAA*
*TAAAAA*CTCGAG

theo-theo-On6
5’CCTAGG*AAACAAACAAA*GCTGTCACCGGATGTGCTTTCCGGTCTGATGAGTCC
GTGTCCATACCAGCATCGATTGATACCAGCATCGTCTTGATGCCCTTGGCAGC
AATTCTTGATGCCCTTGGCAGGGACGGGACGAGGACGAAACAGC*AAAAAGAA*
*AAATAAAAA*CTCGAG

theo-theo-On7
5’CCTAGG*AAACAAACAAA*GCTGTCACCGGATGTGCTTTCCGGTCTGATGAGTCC
GTGTCCATACCAGCATCGGTAAATACCAGCATCGTCTTGATGCCCTTGGCAGT
TGCTCTTGATGCCCTTGGCAGGGACGGGACGAGGACGAAACAGC*AAAAAGAAA*
*AATAAAAA*CTCGAG

theo-theo-On8
5’CCTAGG*AAACAAACAAA*GCTGTCACCGGATGTGCTTTCCGGTCTGATGAGTCC
GTGTCCATACCAGCATCGTTGAATACCAGCATCGTCTTGATGCCCTTGGCAGT
TGATCTTGATGCCCTTGGCAGGGACGGGACGAGGACGAAAACAGC*AAAAAGAA*
*AAATAAAAA*CTCGAG

theo-theo-On9
5’CCTAGG*AAACAAACAAA*GCTGTCACCGGATGTGCTTTCCGGTCTGATGAGTCC
GTGTCCATACCAGCATCGGTTGAATACCAGCATCGTCTTGATGCCCTTGGCAG
TTGATTCTTGATGCCCTTGGCAGGGACGGGACGAGGACGAAACAGC*AAAAAG*
*AAAAATAAAAA*CTCGAG

theo-theo-On10 (Cooperative Buffer gate)
5’CCTAGG*AAACAAACAAA*GCTGTCACCGGATGTGCTTTCCGGTCTGATGAGTCC
GTGTCCATACCAGCATCGGTTGAATACCAGCATCGTCTTGATGCCCTTGGCAG
TTGACTCTTGATGCCCTTGGCAGGGATAGGACGAGGACGAAACAGC*AAAAAG*
*AAAAATAAAAA*CTCGAG

theo-theo-On11 (Cooperative Buffer gate)
5’CCTAGG*AAACAAACAAA*GCTGTCACCGGATGTGCTTTCCGGTCTGATGAGTCC
GTGTCCATACCAGCATCGGTTGAATACCAGCATCGTCTTGATGCCCTTGGCAG
TTGATTCTTGATGCCCTTGGCAGGGATAGGACGAGGACGAAACAGC*AAAAAGA*
*AAAATAAAAA*CTCGAG

theo-theo-On12 (Cooperative Buffer gate)
5’CCTAGG*AAACAAACAAA*GCTGTCACCGGATGTGCTTTCCGGTCTGATGAGTCC
GTGTCCATACCAGCATCGATTGAATACCAGCATCGTCTTGATGCCCTTGGCAG
TTGATTCTTGATGCCCTTGGCAGGGATAGGACGAGGACGAAACAGC*AAAAAGA*
*AAAATAAAAA*CTCGAG

theo-theo-On13 (Cooperative Buffer gate)
5’CCTAGG*AAACAAACAAA*GCTGTCACCGGATGTGCTTTCCGGTCTGATGAGTCC
GTGTCCATACCAGCATCGTGTTATACCAGCATCGTCTTGATGCCCTTGGCAGA
ATGTCTTGATGCCCTTGGCAGGGATAGGACGAGGACGAAACAGC*AAAAAGAAA*
*AATAAAAA*CTCGAG

Two coupled internal Inverter gates responsive to the same input

theo-theo-Off1
5’CCTAGG*AAACAAACAAA*GCTGTCACCGGATGTGCTTTCCGGTCTGATGAGTCC
GTGTTATGATACCAGCATCGACATACCAGCATCGTCTTGATGCCCTTGGCAGG
TTCTTGATGCCCTTGGCAGCATGGACGAGGACGAAACAGC*AAAAAGAAAAATA*
*AAAA*CTCGAG

theo-theo-Off2
5’CCTAGG*AAACAAACAAA*GCTGTCACCGGATGTGCTTTCCGGTCTGATGAGTCC
GTGTTGCTGATACCAGCATCGACATACCAGCATCGTCTTGATGCCCTTGGCAG
GTTCTTGATGCCCTTGGCAGCAGTGGACGAGGACGAAACAGC*AAAAAGAAAAA*
*TAAAAA*CTCGAG

theo-theo-Off3
5’CCTAGG*AAACAAACAAA*GCTGTCACCGGATGTGCTTTCCGGTCTGATGAGTCC
GTGTTATGATACCAGCATCGGACATACCAGCATCGTCTTGATGCCCTTGGCAG
GTTTCTTGATGCCCTTGGCAGCATGGACGAGGACGAAACAGC*AAAAAGAAAAA*
*TAAAAA*CTCGAG

theo-theo-Off4
5’CCTAGG*AAACAAACAAA*GCTGTCACCGGATGTGCTTTCCGGTCTGATGAGTCC
GTGTGTCTGATACCAGCATCGACATACCAGCATCGTCTTGATGCCCTTGGCAG
GTTCTTGATGCCCTTGGCAGCAGGGACGAGGACGAAACAGC*AAAAAGAAAAAT*
*AAAAA*CTCGAG

theo-theo-Off5
5’CCTAGG*AAACAAACAAA*GCTGTCACCGGATGTGCTTTCCGGTCTGATGAGTCC
GTGTGTCCTGATACCAGCATCGGACATACCAGCATCGTCTTGATGCCCTTGGC
AGGTTTCTTGATGCCCTTGGCAGCAGGGACGAGGACGAAACAGC*AAAAAGAAA*
*AATAAAAA*CTCGAG

theo-theo-Off6 (Cooperative Inverter gate)
5’CCTAGG*AAACAAACAAA*GCTGTCACCGGATGTGCTTTCCGGTCTGATGAGTCC
GTGTTATGATACCAGCATCGGCATACCAGCATCGTCTTGATGCCCTTGGCAGG
TTCTTGATGCCCTTGGCAGCATGGACGAGGACGAAACAGC*AAAAAGAAAAATA*
*AAAA*CTCGAG

theo-theo-Off7
5’CCTAGG*AAACAAACAAA*GCTGTCACCGGATGTGCTTTCCGGTCTGATGAGTCC
GTGTTGCTGATACCAGCATCGACATACCAGCATCGTCTTGATGCCCTTGGCAG
GTTCTTGATGCCCTTGGCAGCAGGGACGAGGACGAAACAGC*AAAAAGAAAAAT*
*AAAAA*CTCGAG

theo-theo-Off8
5’CCTAGG*AAACAAACAAA*GCTGTCACCGGATGTGCTTTCCGGTCTGATGAGTCC
GTGTGTTTGATACCAGCATCGACATACCAGCATCGTCTTGATGCCCTTGGCAG
GTTCTTGATGCCCTTGGCAGCAAGGACGAGGACGAAACAGC*AAAAAGAAAAAT*
*AAAAA*CTCGAG

Mutated coupled internal gates

theo-theo-On1M1
5’CCTAGG*AAACAAACAAA*GCTGTCACCGGATGTGCTTTCCGGTCTGATGAGTCC
GTGTCCAGACCAGCATCGTTTATACCAGCATCGTCTTGATGCCCTTGGCAGAA
ATCTTGATGCCTATGGCAGGGACGGGACGAGGACGAAACAGC*AAAAAGAAAAA*
*TAAAAA*CTCGAG

theo-theo-On1M2
5’CCTAGG*AAACAAACAAA*GCTGTCACCGGATGTGCTTTCCGGTCTGATGAGTCC
GTGTCCATACCAGCATCGTTTATACCAGCATCGTCTTGATGCCTATGGCAGAA
ATCTTGATGCCCTTGGCAGGGACGGGACGAGGACGAAACAGC*AAAAAGAAAAA*
*TAAAAA*CTCGAG

theo-theo-On13M1
5’CCTAGG*AAACAAACAAA*GCTGTCACCGGATGTGCTTTCCGGTCTGATGAGTCC
GTGTCCATACCAGCATCGTGTTATACCAGCATCGTCTTGATGCCCTTGGCAGA
ATGTCTTGATGCCTATGGCAGGGATAGGACGAGGACGAAACAGC*AAAAAGAA*
*AAATAAAAA*CTCGAG

theo-theo-On13M2
5’CCTAGG*AAACAAACAAA*GCTGTCACCGGATGTGCTTTCCGGTCTGATGAGTCC
GTGTCCATACCAGCATCGTGTTAGACCAGCATCGTCTTGATGCCTATGGCAGA
ATGTCTTGATGCCCTTGGCAGGGATAGGACGAGGACGAAACAGC*AAAAAGAAA*
*AATAAAAA*CTCGAG

theo-theo-Off2M1
5’CCTAGG*AAACAAACAAA*GCTGTCACCGGATGTGCTTTCCGGTCTGATGAGTCC
GTGTTGCTGAGACCAGCATCGACATACCAGCATCGTCTTGATGCCCTTGGCAG
GTTCTTGATGCCTATGGCAGCAGTGGACGAGGACGAAACAGC*AAAAAGAAAAA*
*TAAAAA*CTCGAG

theo-theo-Off2M2
5’CCTAGG*AAACAAACAAA*GCTGTCACCGGATGTGCTTTCCGGTCTGATGAGTCC
GTGTTGCTGATACCAGCATCGACATACCAGCATCGTCTTGATGCCTATGGCAG
GTTCTTGATGCCCTTGGCAGCAGTGGACGAGGACGAAACAGC*AAAAAGAAAAA*
*TAAAAA*CTCGAG

theo-theo-Off6M1
5’CCTAGG*AAACAAACAAA*GCTGTCACCGGATGTGCTTTCCGGTCTGATGAGTCC
GTGTTATGAACCCAGCATCGGCATACCAGCATCGTCTTGATGCCCTTGGCAGG
TTCTTGATGCCTATGGCAGCATGGACGAGGACGAAACAGC*AAAAAGAAAAATA*
*AAAA*CTCGAG

theo-theo-Off6M2

5’CCTAGG*AAACAAACAAA*GCTGTCACCGGATGTGCTTTCCGGTCTGATGAGTCC
GTGTTATGATACCAGCATCGGCATACCAGCATCGTCTTGATGCCTATGGCAGG
TTCTTGATGCCCTTGGCAGCATGGACGAGGACGAAACAGC*AAAAAGAAAAATA*
*AAAA*CTCGAG

AND gate

L2bulge9 + L2bulge1tc

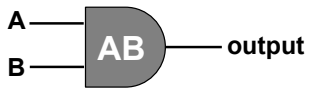

A theo	B tc	output GFP
0	0	0
0	1	0
1	0	0
1	1	1

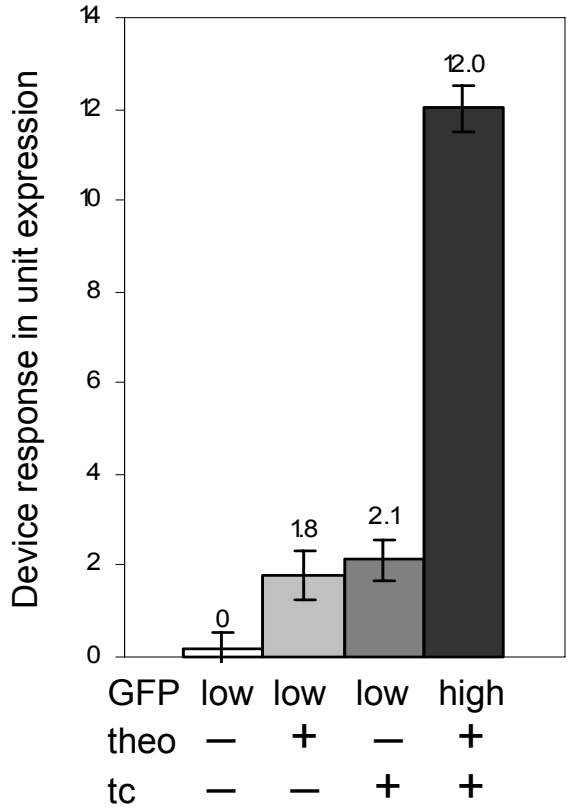

Figure S1. The device response and truth table of an AND gate (L2bulge9+L2bulge1tc) based on SI 1.2. The RNA device is constructed by coupling a theophylline-responsive Buffer gate (L2bulge9) and a tetracycline-responsive Buffer gate (L2bulge1tc) in the 3' UTR of a target transcript. Device response under different input conditions (theo or tc (-), 0 mM; theo (+), 5 mM; tc (+), 0.5 mM) is reported as the difference between gene expression activity in the absence of both inputs and that at the indicated input conditions.

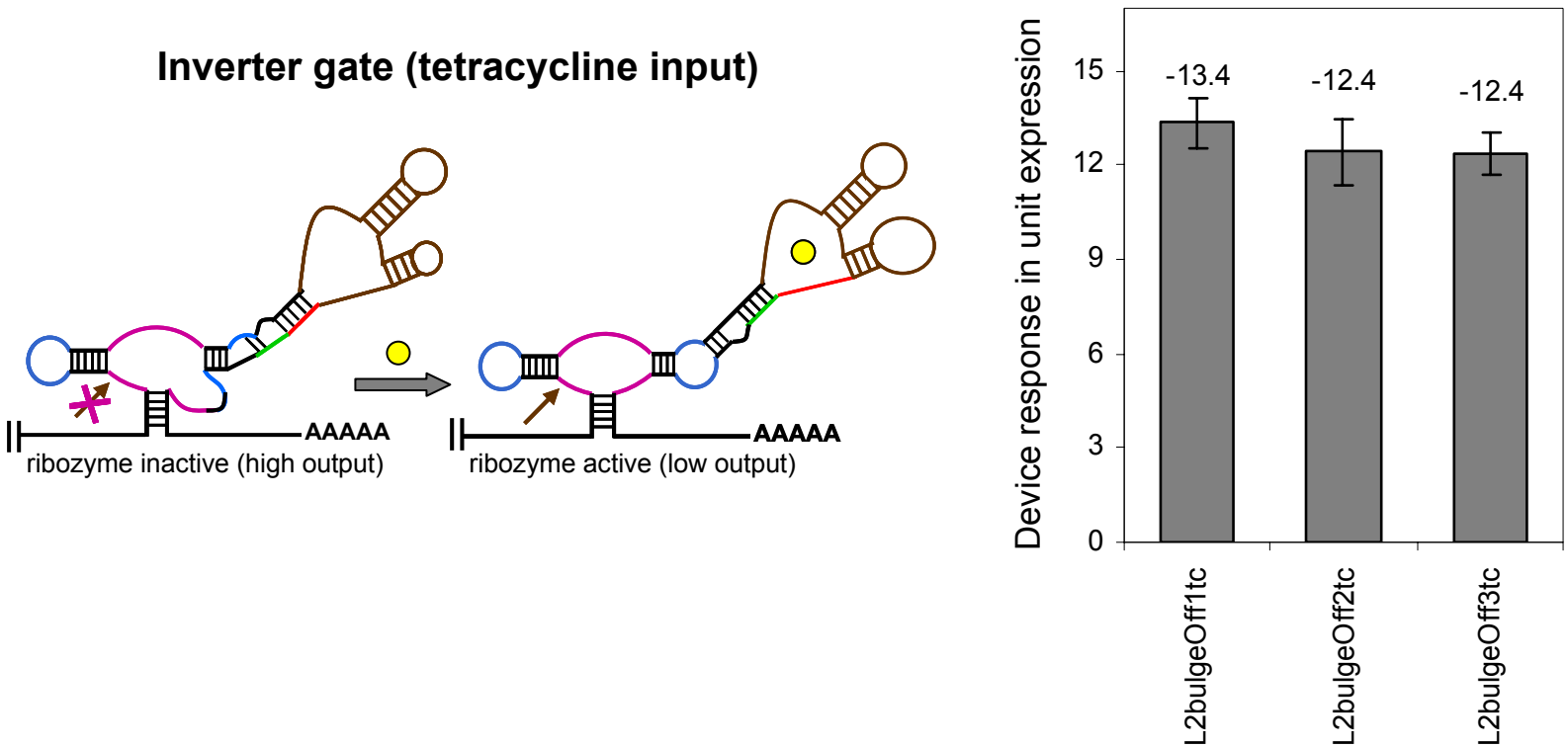

Figure S2. Schematic representation and device response of tetracycline-responsive Inverter gates. The color scheme follows that described in **Fig. 1**. Device response is reported as the difference between expression activities in the absence and presence of 0.5 mM tetracycline. The negative sign indicates the down-regulation of target gene expression by the Inverter gates.

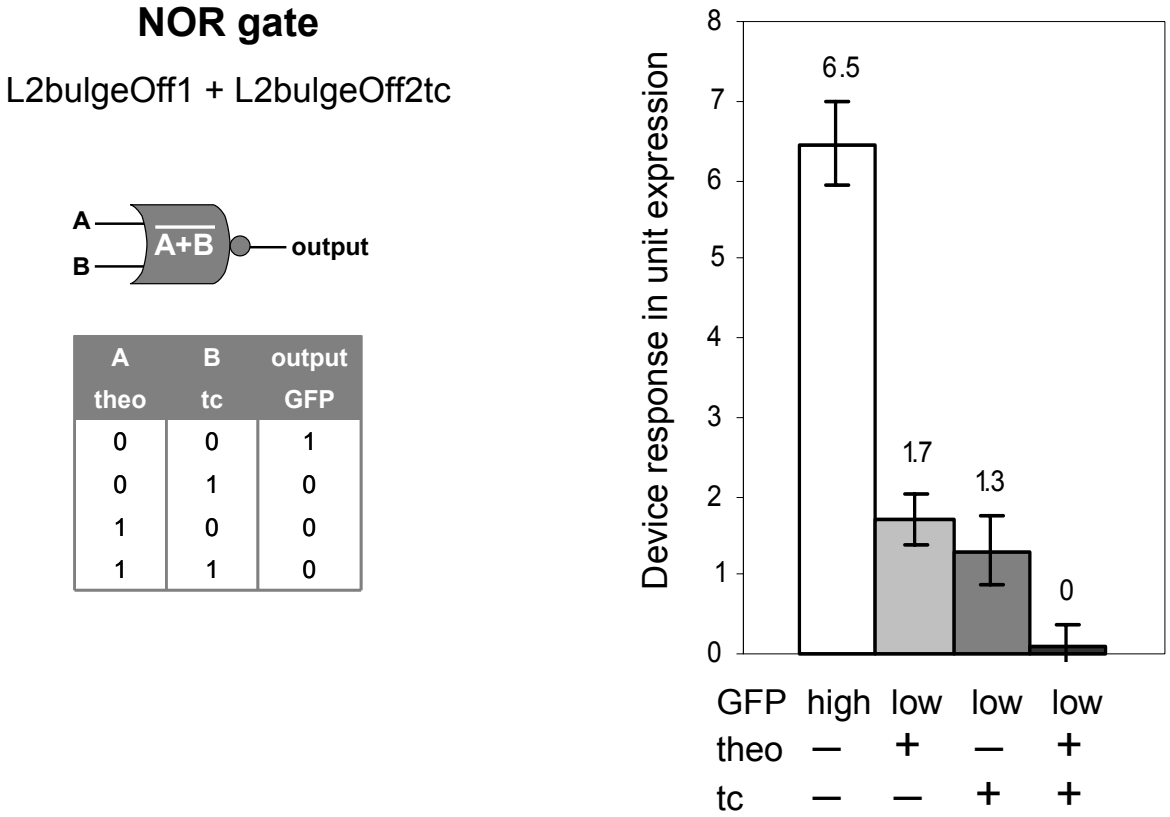

Figure S3. The device response and truth table of a NOR gate (L2bulgeOff1+L2bulgeOff2tc) based on SI 1.3. The RNA device is constructed by coupling a theophylline-responsive Inverter gate (L2bulgeOff1) and a tetracycline-responsive Inverter gate (L2bulgeOff2tc) in the 3' UTR of a target transcript. Device response under different input conditions (theo or tc (-), 0 mM; theo (+), 10 mM; tc (+), 0.5 mM) is reported as the difference between expression activity in the presence of both inputs and that at the indicated input conditions.

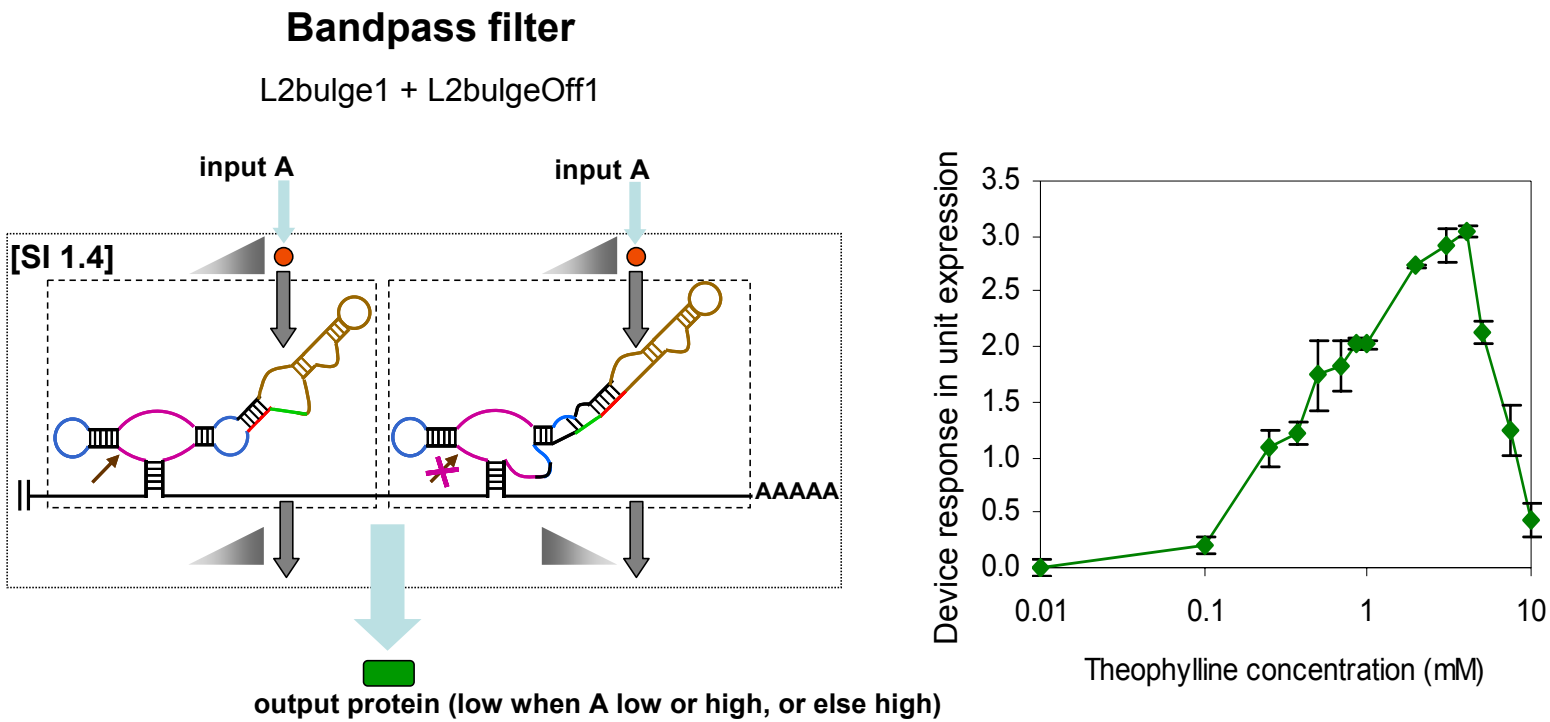

Figure S4. Schematic representation and device response of a bandpass filter (L2bulge1+L2bulgeOff1) based on SI 1.4. The color scheme follows that described in **Fig. 1**. Single-input gates are indicated in dashed boxes, and triangles indicate relationships between associated gate inputs and outputs. The RNA device is constructed by coupling a theophylline-responsive Buffer gate (L2bulge1) and a theophylline-responsive Inverter gate (L2bulgeOff1) in the 3' UTR of a target transcript. Device response is reported as the difference between expression activities in the absence and presence of theophylline .

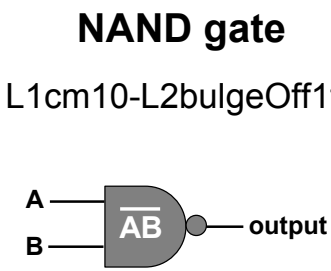

A	B	output
theo	tc	GFP
0	0	1
0	1	1
1	0	1
1	1	0

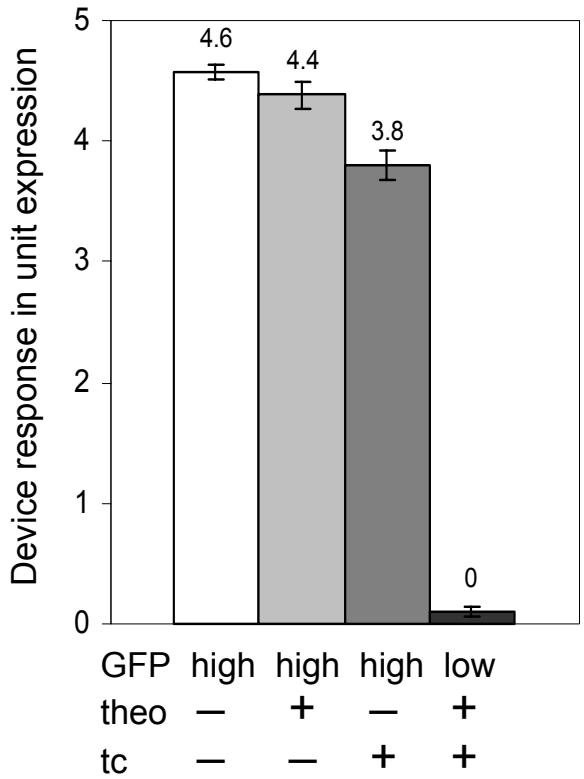

Figure S5. The device response and truth table of a NAND gate (L1cm10-L2bulgeOff1tc) based on SI 2.1. The RNA device is constructed by coupling a theophylline-responsive internal Inverter gate (L1cm10) and a tetracycline-responsive internal Inverter gate (L2bulgeOff1tc) to stems I and II, respectively, of a ribozyme. Device response under different input conditions (theo or tc (-), 0 mM; theo (+), 10 mM; tc (+), 1 mM) is reported as the difference between expression activity in the presence of both inputs and that at the indicated input conditions.

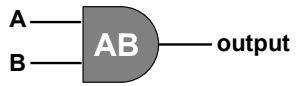

A theo	B tc	output GFP
0	0	0
0	1	0
1	0	0
1	1	1

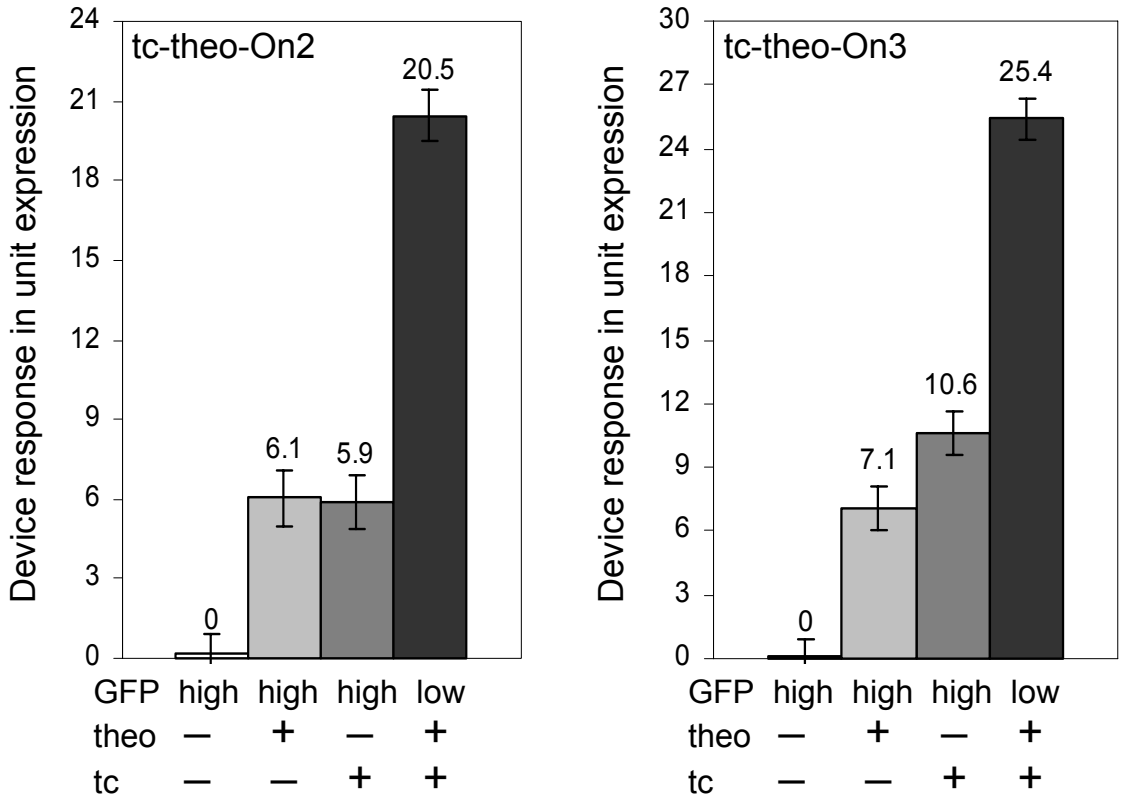

Figure S6. The device response and truth table of AND gates (tc-theo-On2 and tc-theo-On3) based on SI 3.1. The RNA devices are constructed by coupling a theophylline-responsive internal Buffer gate (IG1) and a tetracycline-responsive internal Inverter gate (IG2) to stem II of a ribozyme. Device response under different input conditions (theo or tc (-), 0 mM; theo (+), 2.5 mM; tc (+), 0.5 mM) is reported as the difference between expression activity in the absence of both inputs and that at the indicated input conditions.

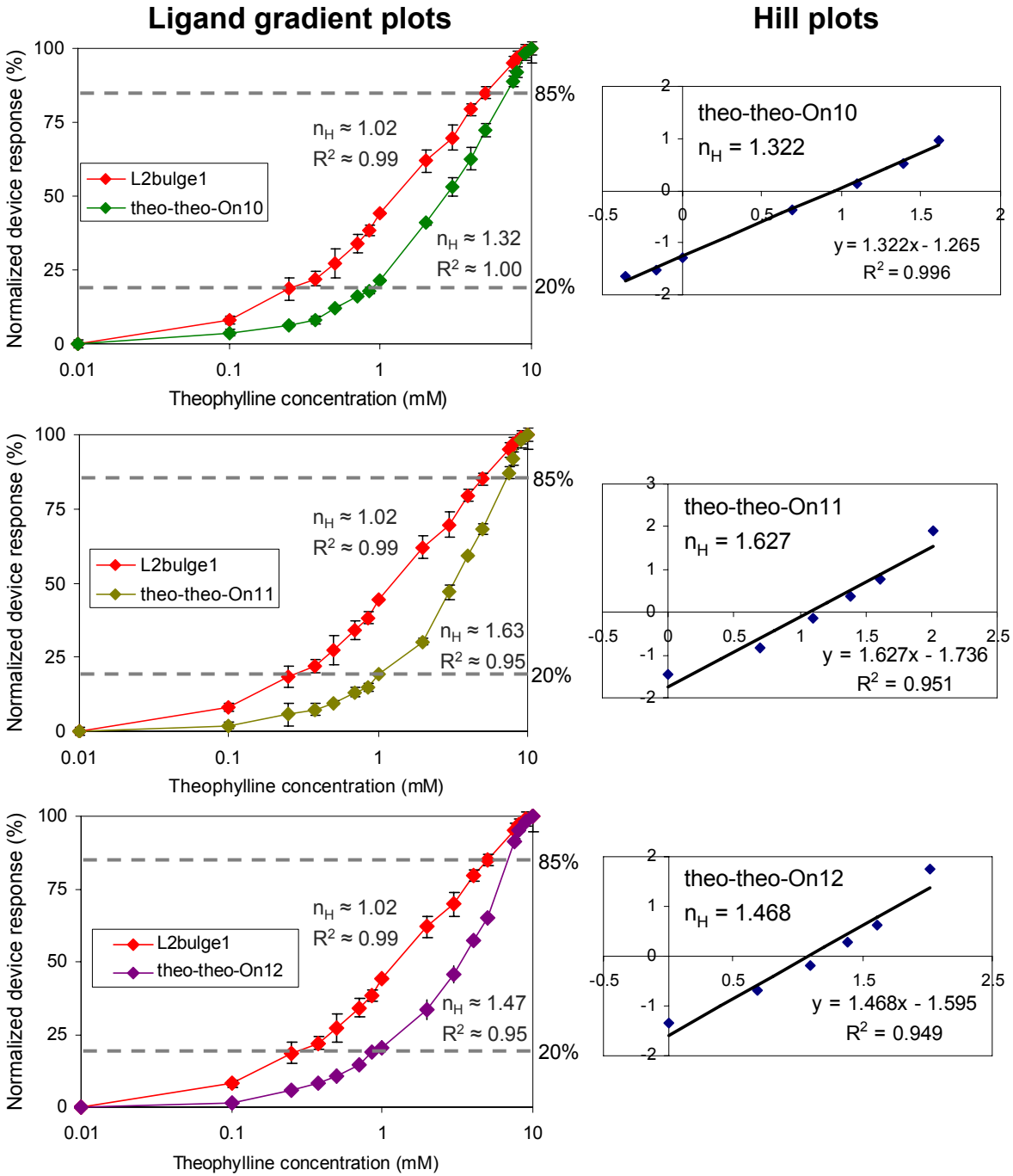

Figure S7. The device response over varying theophylline concentrations of RNA devices composed of internal Buffer and Inverter gates (theo-theo-On10 – 12) and their single-internal gate device counterpart (L2bulge1) demonstrates programmed cooperativity. The device response is normalized to the response at 10 mM theophylline. Corresponding Hill plots are constructed for 20-85% of each normalized device response by plotting log [fraction expressed / (1 - fraction expressed)] against log [input concentration], where the slope represents the Hill coefficient (n_H).

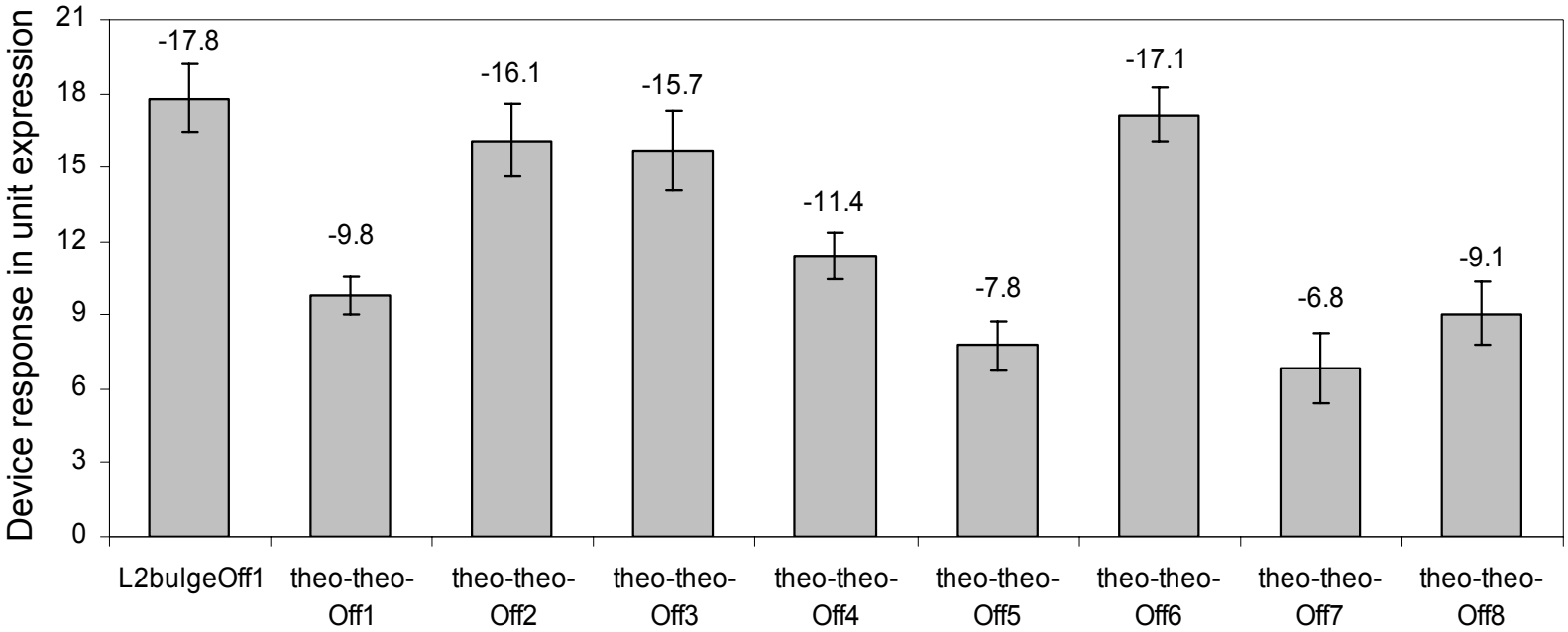

Figure S8. The device response of RNA devices composed of two internal Inverter gates and their single-internal gate device counterpart (L2bulgeOff1). The RNA devices are constructed by coupling two theophylline-responsive internal Inverter gates (IG1, IG2) to stem II of a ribozyme. Device response is reported as the difference between expression activities in the absence and presence of 10 mM theophylline. The negative sign indicates the down-regulation of target gene expression. While all eight devices performed Inverter operations like L2bulgeOff1, only one (theo-theo-Off6) exhibited a low degree of programmed cooperativity (see fig. S9).

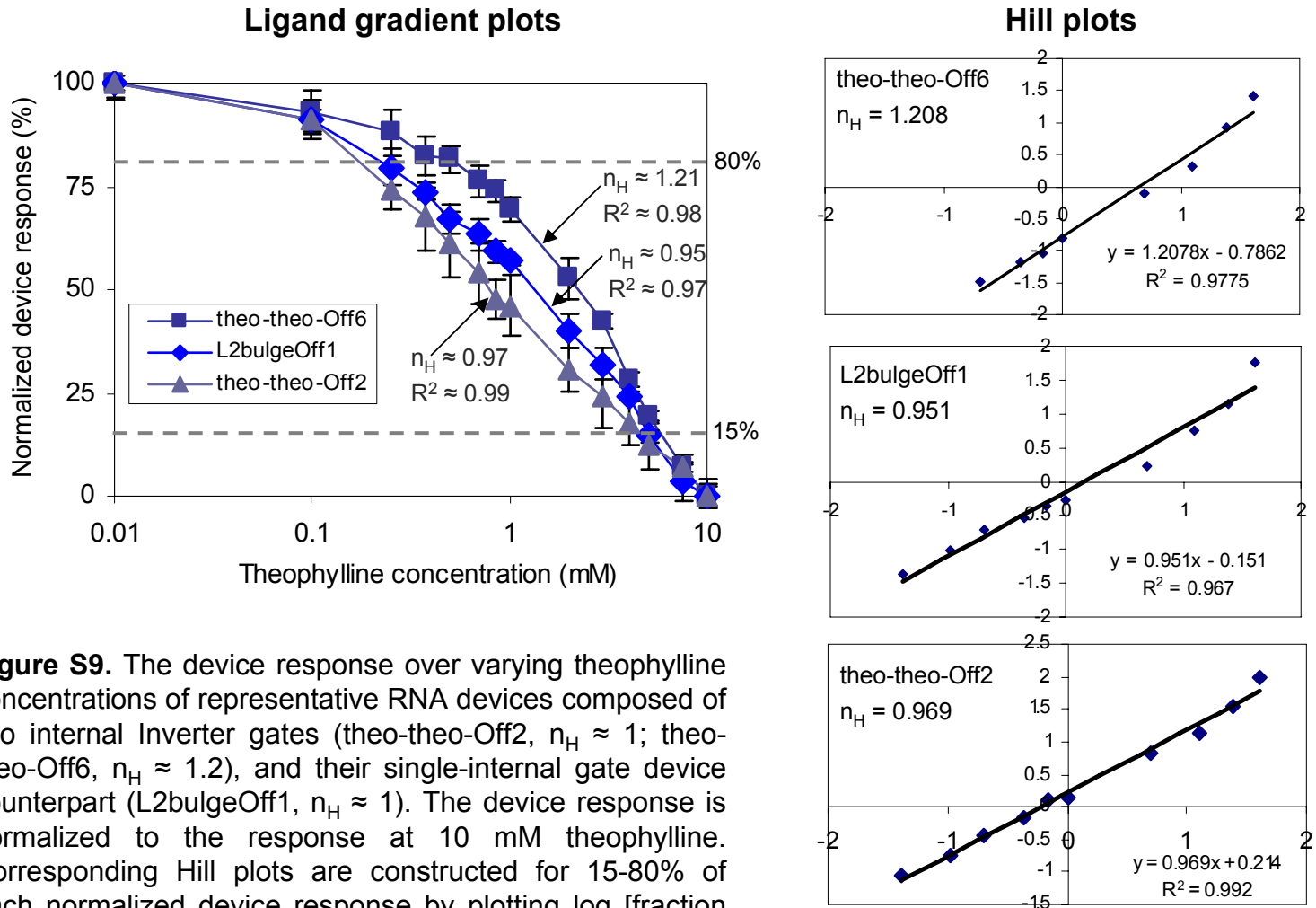

Figure S9. The device response over varying theophylline concentrations of representative RNA devices composed of two internal Inverter gates (theo-theo-Off2, $n_H \approx 1$; theo-theo-Off6, $n_H \approx 1.2$), and their single-internal gate device counterpart (L2bulgeOff1, $n_H \approx 1$). The device response is normalized to the response at 10 mM theophylline. Corresponding Hill plots are constructed for 15-80% of each normalized device response by plotting log [fraction repressed / (1 - fraction repressed)] against log [input concentration], where the slope represents the Hill coefficient (n_H).

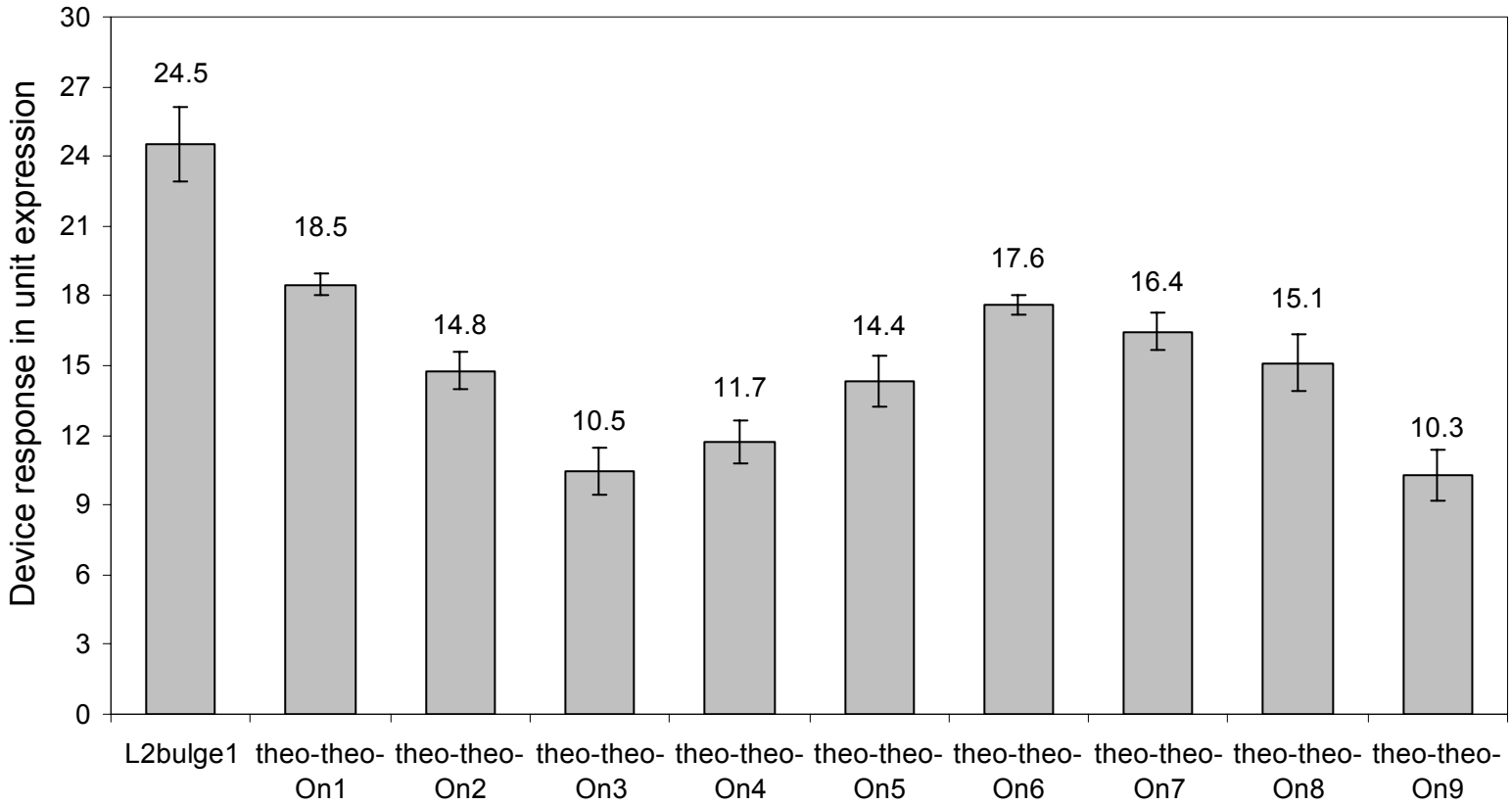

Figure S10. The device response of RNA devices composed of internal Buffer and Inverter gates and their single-internal gate device counterpart (L2bulge1). The RNA devices are constructed by coupling theophylline-responsive internal Buffer (IG1) and Inverter (IG2) gates to stem II of a ribozyme. Device response is reported as the difference between expression activities in the absence and presence of 10 mM theophylline. While all nine devices performed Buffer operations like L2bulge1, none of them exhibited programmed cooperativity where $\Delta\Delta G_{IG1}$ = 0.3 kcal/mol was used. In contrast, when $\Delta\Delta G_{IG1}$ was increased to 1 kcal/mol, the devices exhibited substantial degrees of cooperativity (see Fig. 4E and fig. S7), indicating that $\Delta\Delta G_{IG1}$ was important to the observed cooperative response.

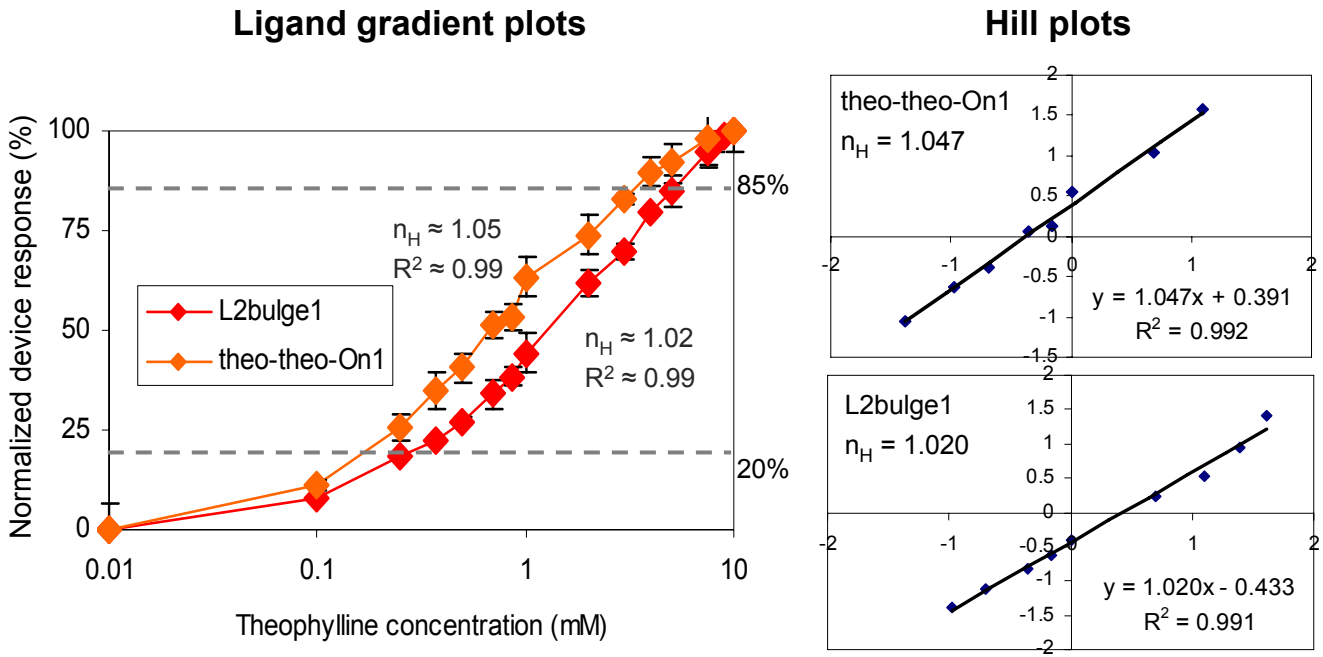

Figure S11. The device response over varying theophylline concentrations of a representative RNA device composed of internal Buffer and Inverter gates (theo-theo-On1) and its single-internal gate device counterpart (L2bulge1) demonstrates no programmed cooperativity ($n_H \approx 1$). The device response is normalized to the response at 10 mM theophylline. Corresponding Hill plots are constructed for 20-85% of each normalized device response by plotting log [fraction expressed / (1 - fraction expressed)] against log [input concentration], where the slope represents the Hill coefficient (n_H).

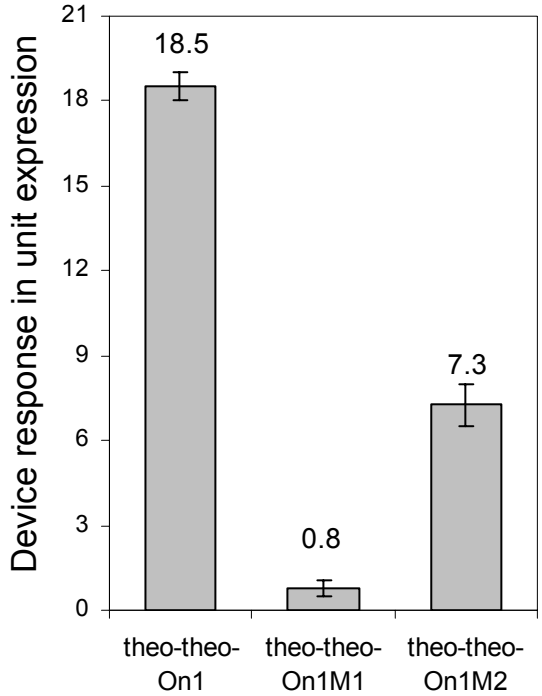

Figure S12. The device response of a representative RNA device composed of internal Buffer and Inverter gates (theo-theo-On1) and its mutated sensor variants demonstrates that input binding at both internal gates is responsible for the overall device response. Theo-theo-On1M1, mutation to the sensor in IG1; theo-theo-On1M2, mutation to sensor in IG2. Device response is reported as the difference in expression activities in the absence and presence of 10 mM theophylline. Individual mutations in both internal gates exhibited considerably lower output levels, supporting that both internal gates contribute to the overall device response. However, it was observed that theo-theo-On1M2 demonstrated less inhibition of device response compared to theo-theo-On1M1. The mutation of IG1 is anticipated to have a more significant impact on device performance as the device response is directly regulated by IG1.

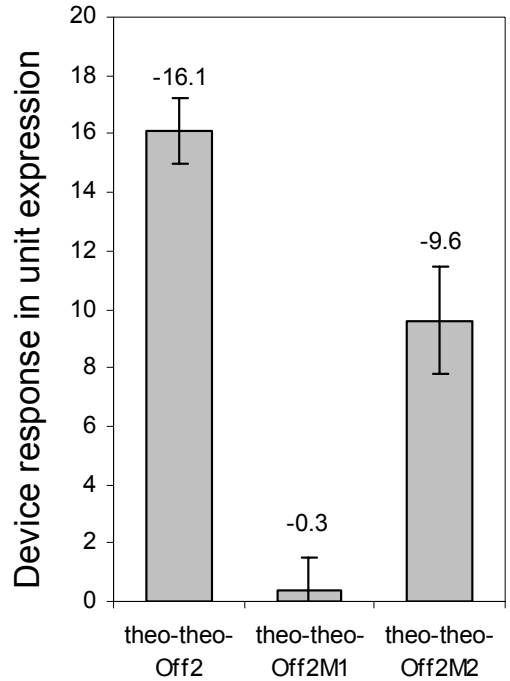

Figure S13. The device response of a representative RNA device composed of two internal Inverter gates (theo-theo-Off2) and its mutated sensor variants demonstrates that input binding at both internal gates is responsible for the overall device response. Theo-theo-Off2M1, mutation to the sensor in IG1; theo-theo-Off2M2, mutation to sensor in IG2. Device response is reported as the difference in expression activities in the absence and presence of 10 mM theophylline. The negative sign indicates the down-regulation of target gene expression. The mutation of IG1 is anticipated to have a more significant impact on device performance as the device response is directly regulated by IG1.

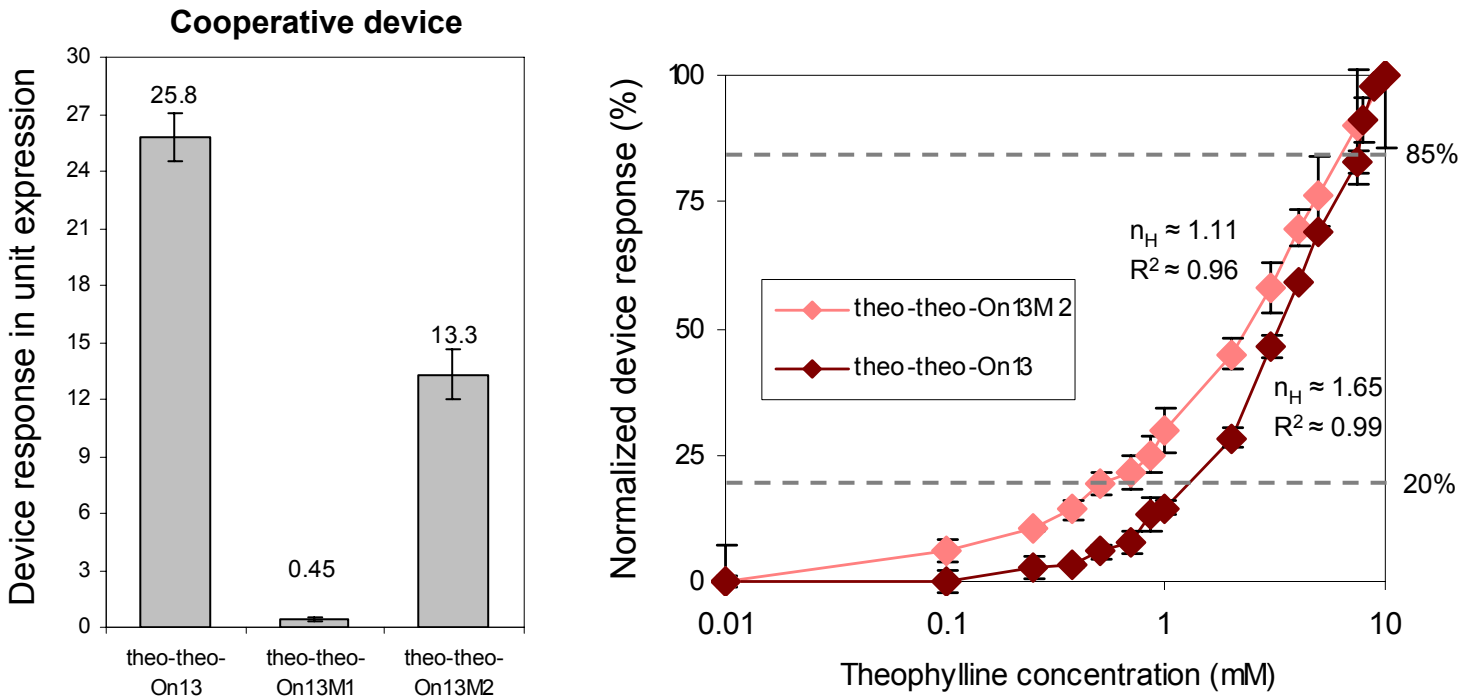

Figure S14. The device response of a representative RNA device composed of internal Buffer and Inverter gates that exhibits programmed cooperativity (theo-theo-On13) and its mutated sensor variants demonstrates that input binding at both internal gates is responsible for the overall device response. Theo-theo-On13M1, mutation to the sensor in IG1; theo-theo-On13M2, mutation to sensor in IG2. Device response is reported as the difference in expression activities in the absence and presence of 10 mM theophylline. The device response is normalized to the response at 10 mM theophylline. Corresponding Hill plots are constructed for 20-85% of each normalized device response by plotting log [fraction expressed / (1 - fraction expressed)] against log [input concentration], where the slope represents the Hill coefficient (n_H). The mutation of IG1 is anticipated to have a more significant impact on device performance as the device response is directly regulated by IG1.

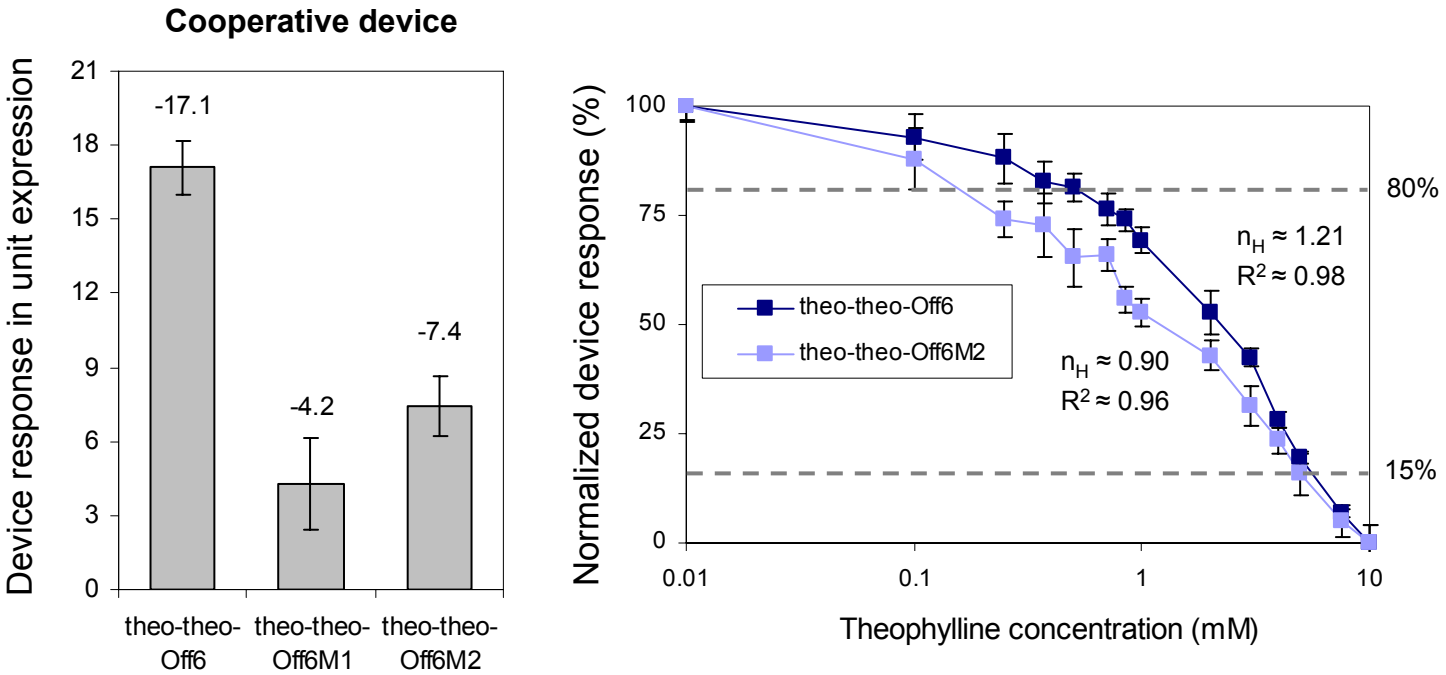

Figure S15. The device response of a representative RNA device composed of two internal Inverter gates that exhibits programmed cooperativity (theo-theo-Off6) and its mutated sensor variants demonstrates that input binding at both internal gates is responsible for the overall device response. Theo-theo-Off6M1, mutation to the sensor in IG1; theo-theo-Off6M2, mutation to sensor in IG2. Device response is reported as the difference between expression activities in the absence and presence of 10 mM theophylline. The negative sign indicates the down-regulation of target gene expression. The device response is normalized to the response at 10 mM theophylline. Corresponding Hill plots are constructed for 15-80% of each normalized device response by plotting log [fraction repressed / (1 - fraction repressed)] against log [input concentration], where the slope represents the Hill coefficient (n_H). The mutation of IG1 is anticipated to have a more significant impact on device performance as the device response is directly regulated by IG1.

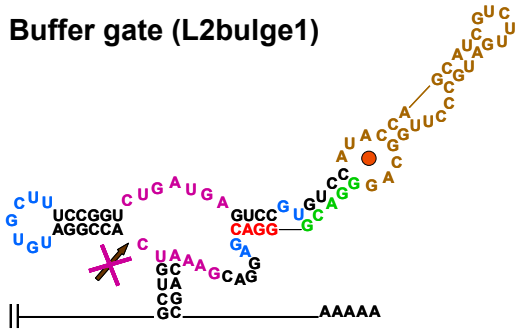

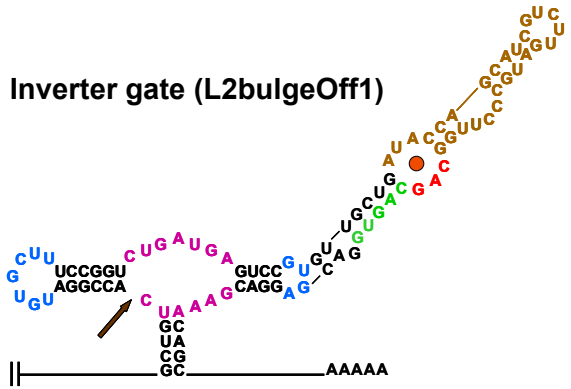

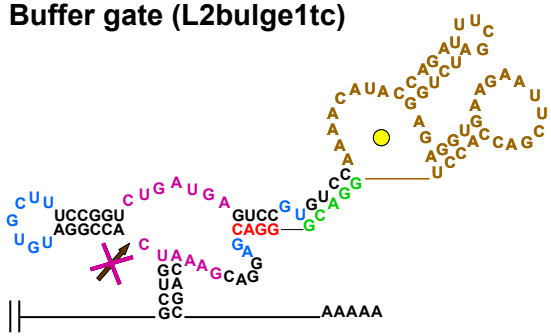

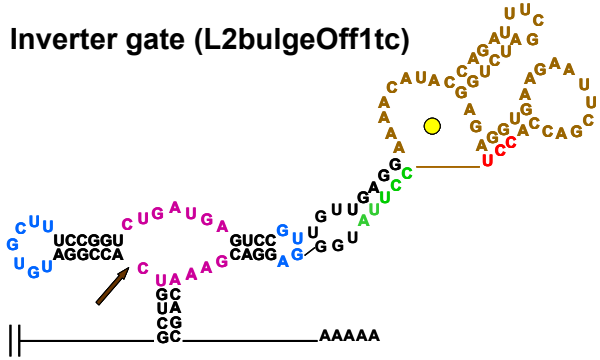

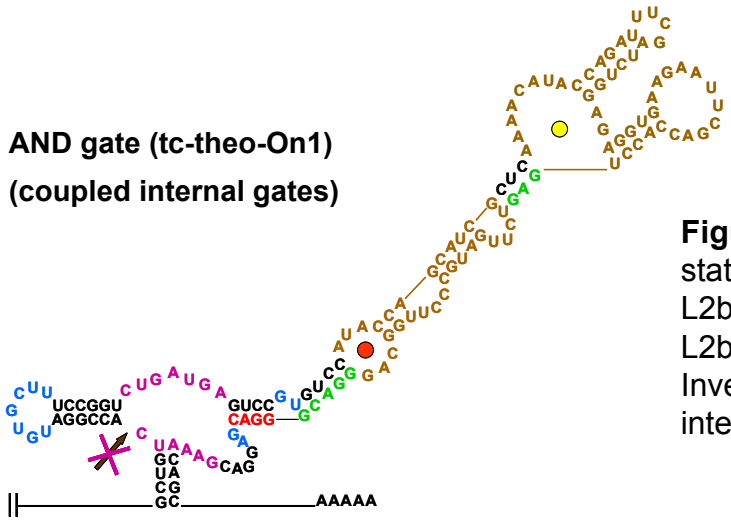

Figure S16. Secondary structures and sequences of input-bound states of representative RNA devices. Single-input Buffer gates: L2bulge1, L2bulge1tc; single-input Inverter gates: L2bulgeOff1, L2bulgeOff1tc; RNA device composed of internal Buffer (IG1) and Inverter (IG2) gates responsive to different inputs, illustrating points of integration of two sensor-transmitter components: tc-theo-On1.

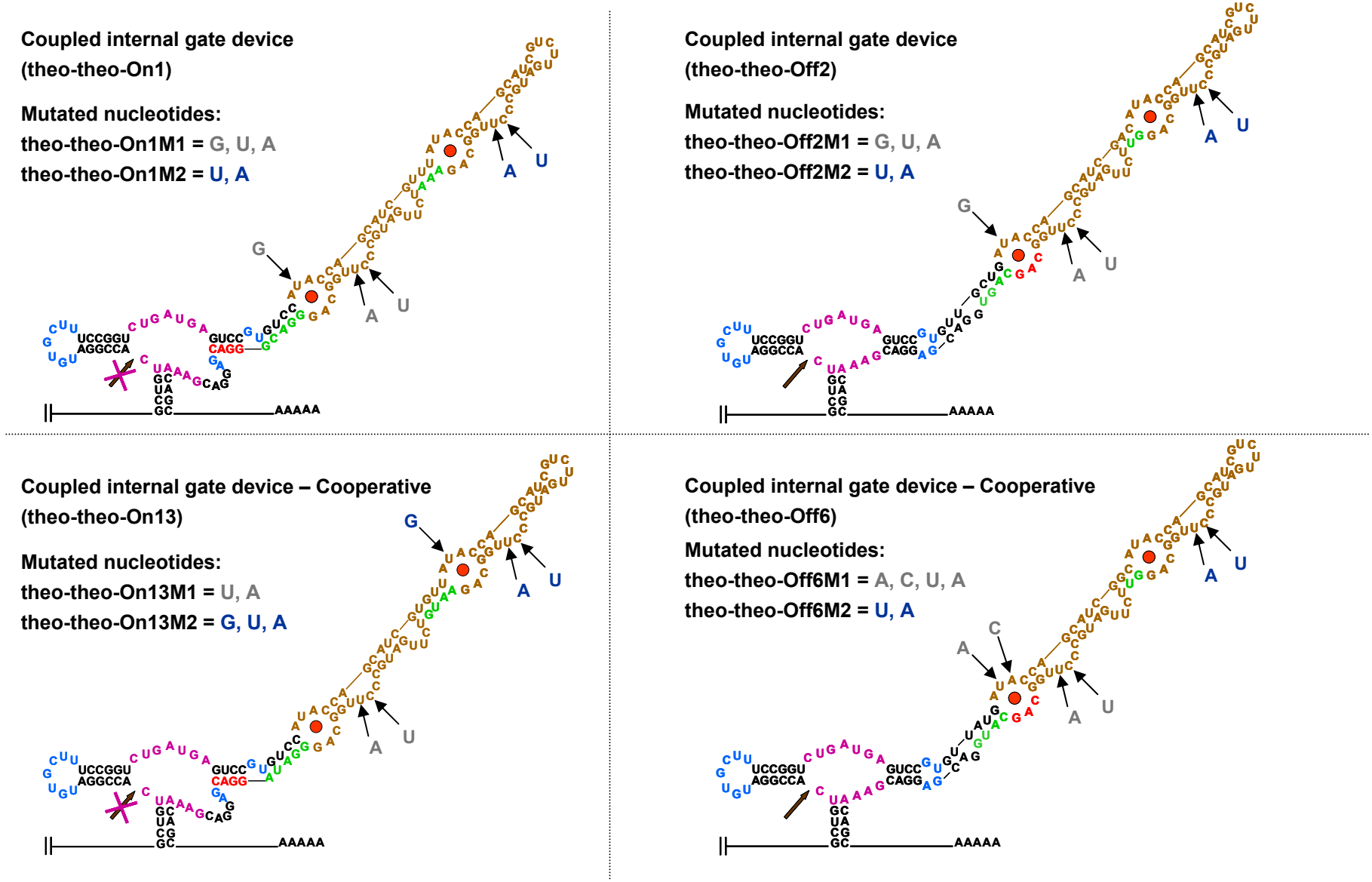

Figure S17. Secondary structures and sequences of input-bound states of representative RNA device composed of internal Buffer and Inverter gates responsive to the same input, illustrating points of integration of two sensor-transmitter components. Nucleotides that were altered in the mutational studies are indicated for the sensors in IG1 and IG2. RNA devices that do not exhibit programmed cooperativity: theo-theo-On1, theo-theo-Off2; RNA devices that exhibit programmed cooperativity: theo-theo-On13, theo-theo-Off6.

Table S1. The basal output signals and device signals of the RNA devices studied in this work are shown over the full transcriptional range of the employed promoter. The predicted basal output signals of coupled devices based on the appropriate single-input gate response(s) and independent function are also reported. Predicted signals that do not match the measured output signals are indicated in italics.

Device	Device signal (%) (over the full transcriptional range)				Predicted basal signal (%) for coupled devices
	theo, tc (-)	theo (+)	tc (+)	theo, tc (+)	
SI 1.1					
L2bulge1tc (Buffer-tc)	37		96		
2xL2bulge1tc (2xBuffer-tc)	16		46		14
L2bulge1 (Buffer1)	40	89			
2xL2bulge1 (2xBuffer1)	20	37			16
L2bugle8 (Buffer8)	12	48			
2xL2bulge8 (2xBuffer8)	7	19			1
L2bulge5 (Buffer5)	82	100			
L2bulge1+L2bulge5 (Buffer1+Buffer5)	25	43			33
L2bulgeOff1 (Inverter1)	62	26			
2xL2bulgeOff1 (2xInverter1)	37	21			38
L2cm4 (Inverter4)	78	41			
2xL2cm4 (2xInverter4)	32	20			*61*
L2bulgeOff1+L2cm4 (Inverter1+Inverter4)	31	17			*48*
tc-responsive Inverter gates					
L2bulgeOff1tc (Inverter)	39		12		
L2bulgeOff2tc (Inverter)	42		17		
L2bulgeOff3tc (Inverter)	42		17		
SI 1.2 (AND gate)					
L2bulge1+L2bulge1tc	18	22	24	46	15
L2bulge9+L2bulge1tc	12	15	16	36	11
L2bulge9 (single-input Buffer)	30	72			
SI 1.3 (NOR gate)					
L2bulgeOff1+L2bulgeOff1tc	27	15	13	11	24
L2bulgeOff1+L2bulgeOff2tc	28	18	17	15	26
SI 2.1 (NAND gate)					
L1cm10+L2bulgeOff3tc	54	52	55	43	
L1cm10+L2bulgeOff1tc	51	51	50	42	

Table S1 (continued)

Device	Device signal (%) (over the full transcriptional range)			
	theo, tc (-)	theo (+)	tc (+)	theo, tc (+)
SI 3.1 (AND gate)				
tc-theo-On1	36	48	50	89
tc-theo-On2	39	51	51	80
tc-theo-On3	39	53	61	90
SI 3.2 (dual sensor-transmitter)				
Buffer function				
theo-theo-On1	36	73		
theo-theo-On2	41	70		
theo-theo-On3	54	75		
theo-theo-On4	66	89		
theo-theo-On5	69	98		
theo-theo-On6	46	81		
theo-theo-On7	42	75		
theo-theo-On8	31	61		
theo-theo-On9	23	44		
theo-theo-On10 (cooperative)	16	54		
theo-theo-On11 (cooperative)	13	55		
theo-theo-On12 (cooperative)	12	60		
theo-theo-On13 (cooperative)	23	75		
Inverter function				
theo-theo-Off1	34	15		
theo-theo-Off2	60	27		
theo-theo-Off3	67	36		
theo-theo-Off4	47	24		
theo-theo-Off5	40	24		
theo-theo-Off6 (cooperative)	58	24		
theo-theo-Off7	54	40		
theo-theo-Off8	43	24		
SI 3.3 (OR gate)				
tc/theo-On1	48	65	64	72
tc/theo-On2	42	60	62	71

Table S2. Free energy changes associated with RNA devices composed of internal Buffer and Inverter gates and associated Hill coefficients. Free energy changes between RNA device states are predicted from a standard RNA folding program, RNAStructure 4.2.

Device	$\Delta\Delta G_{IG2}$ (kcal / mol)	$\Delta\Delta G_{IG1}$ (kcal / mol)	Degree of programmed cooperativity
Non-cooperative			
theo-theo-On1	0.3	0.3	none
theo-theo-On2	2.8	0.3	none
theo-theo-On3	1.8	0.3	none
theo-theo-On4	1.9	0.3	none
theo-theo-On5	0.0	0.3	none
theo-theo-On6	0.9	0.3	none
theo-theo-On7	3.0	0.3	none
theo-theo-On8	2.8	0.3	none
theo-theo-On9	2.9	0.0	none
Cooperative			
theo-theo-On10	0.3	1.0	$n_H \approx 1.32$
theo-theo-On11	1	1.0	$n_H \approx 1.63$
theo-theo-On12	1.4	1.0	$n_H \approx 1.47$
theo-theo-On13	2.2	1.0	$n_H \approx 1.65$

Supporting Online References

S1. J. Sambrook, D. W. Russell, *Molecular cloning: a laboratory manual* (Cold Spring Harbor Laboratory Press, Cold Spring Harbor, NY, ed. 3, 2001).
S2. C. Mateus, S. V. Avery, *Yeast* **16**, 1313 (2000).
S3. M. N. Win, C. D. Smolke, *Proc Natl Acad Sci U S A* **104**, 14283 (2007).
S4. R. Gietz, R. Woods, in *Guide to Yeast Genetics and Molecular and Cell Biology, Part B,* C. Guthrie, G. Fink, Eds. (Academic Press, San Diego, 2002), vol. 350, pp. 87-96.
S5. Y. Yokobayashi, R. Weiss, F. H. Arnold, *Proc Natl Acad Sci U S A* **99**, 16587 (2002).
S6. S. Basu, R. Mehreja, S. Thiberge, M. T. Chen, R. Weiss, *Proc Natl Acad Sci U S A* **101**, 6355 (2004).
S7. E. Levine, Z. Zhang, T. Kuhlman, T. Hwa, *PLoS Biol* **5**, e229 (2007).
S8. S. S. Hebert *et al.*, *Proc Natl Acad Sci U S A* **105**, 6415 (2008).
S9. G. A. Calin *et al.*, *Proc Natl Acad Sci U S A* **105**, 5166 (2008).
S10. A. Ventura *et al.*, *Cell* **132**, 875 (2008).
S11. R. Welz, R. R. Breaker, *RNA* **13**, 573 (2007).
S12. G. A. Soukup, G. A. Emilsson, R. R. Breaker, *J Mol Biol* **298**, 623 (2000).
S13. D. A. Rodionov, I. Dubchak, A. Arkin, E. Alm, M. S. Gelfand, *Genome Biol* **5**, R90 (2004).
S14. K. Rinaudo *et al.*, *Nat Biotechnol* **25**, 795 (2007).
S15. T. L. Deans, C. R. Cantor, J. J. Collins, *Cell* **130**, 363 (2007).